Research Square

Preprints are preliminary reports that have not undergone peer review.
They should not be considered conclusive, used to inform clinical practice,
or referenced by the media as validated information.

Geopolymer-Bound Recycled Waste Glass Aggregate Composite Columns for Ground Improvement

K. K.W. Premathilaka
Integra Consultants
D. S. Liyanapathirana
s.liyanapathirana@westernsydney.edu.au
Western Sydney University
C. J. Leo
Western Sydney University
Pan Hu
Western Sydney University

Research Article

Keywords: recycled waste glass aggregates, geopolymer, waste Aluminium, strain softening, column-supported embankments, finite element method

Posted Date: November 18th, 2026

DOI: https://doi.org/10.21203/rs.3.rs-11631013/v1

License: This work is licensed under a Creative Commons Attribution 4.0 International License.
Read Full License

Additional Declarations: No competing interests reported.

Geopolymer-Bound Recycled Waste Glass Aggregate Composite Columns for Ground Improvement

K.K.W. Prematilaka, PhD
Senior Geotechnical Engineer
Integra Consultants, Rosebery, NSW, Australia 2018
Email: wpremathilaka@integraconsultants.com.au
ORCID 0000-0001-6732-1552

D.S. Liyanapathirana*, PhD, FIEAust, F.ASCE
Professor of Geotechnical Engineering
School of Engineering, Western Sydney University, NSW, Australia 2747
Email: s.liyanapathirana@westernsydney.edu.au
*Corresponding author
ORCID 0000-0002-7239-6089

C.J. Leo, PhD
Emeritus Professor of Geotechnical Engineering
School of Engineering, Western Sydney University, NSW, Australia 2747
Email: c.leo@westernsydney.edu.au
ORCID 0000-0003-4242-9545

Pan Hu, PhD
Senior Lecturer
School of Engineering, Western Sydney University, NSW, Australia 2747
Email: p.hu@westernsydney.edu.au
ORCID 0000-0002-3903-1125

Abstract

This paper presents a novel composite material with recycled waste glass aggregates bound by a geopolymer, developed by combining waste materials, for ground improvement. An extension of the Mohr-Coulomb constitutive model is proposed to simulate the experimentally observed behaviour of the geopolymer-bound recycled waste glass composite (GRWGC). A case study of soft ground reinforced with stone columns in Brazil was used to examine the effectiveness of the proposed methodology with glass aggregates as a substitute for conventional stone columns, where the long-term stability of unbound aggregate columns can be adversely affected by the low lateral confinement provided by the surrounding soft soil. Three-dimensional (3D) coupled mechanical and hydraulic finite element simulations were performed for both stone and proposed GRWGC columns. Significant reductions in settlements and lateral displacements were observed when GRWGC columns were used with the same spacing as in the case study. A 3D parametric study was conducted to investigate the performance of GRWGC column-supported embankments by varying the key design parameters and the performance of the proposed ground improvement method is evaluated by comparing: (i) stress concentration ratio, (ii) arching ratio, (iii) settlement (iv) differential settlement, (v) lateral displacement and (vi) geogrid tension. The impact of each key design parameter on the overall performance of GRWGC column-supported embankments is ranked using an influencing factor, which can be used as a design guideline for the proposed ground improvement method.

keywords: recycled waste glass aggregates, geopolymer, waste Aluminium, strain softening, column-supported embankments, finite element method.

1. Introduction

Stone columns are among the most time-efficient and economical ground improvement methods used globally. The earliest recorded use of stone columns for ground improvement dates back to France in 1839 (Castro 2017). However, the technique did not gain widespread recognition in Europe until the early 1960s, when the use of granular materials for soil reinforcement became more prevalent. Due to its effectiveness, the method rapidly expanded across the globe, becoming a well-established ground improvement practice (Ambily and Gandhi 2007). The soil strength gain with accelerated consolidation is one of the key features of the stone column-based soft ground improvement, in addition to the ground reinforcement (Mitchell and Huber 1985). The poor performance of stone columns with unbound aggregates in weak ground conditions with low lateral support can be recognised as one of the main drawbacks of this method, causing low stability and bulging failure of columns (Balaam and Booker 1981; Hugher and Withers 1974). Extensive research has been conducted to improve the bearing capacity of soft ground with stone columns, and the proposed solutions can be classified into three categories: (i) reinforcement (Black et al. 2007; Dutta et al. 2012; Shivashankar et al. 2010), (ii) encasement (Castro and Sagaseta 2011; Malarvizhi 2007) and (iii) cementation (Dheerendra Babu et al. 2013; Liu et al. 2015) of the most vulnerable sections of stone columns.

In modern sustainability-focused construction practices, environmental and social concerns associated with natural aggregate production have become a key focus. Various sustainable material options were explored as alternatives to natural aggregates in stone columns. Recycled aggregates (Foda et al. 2024; Shahverdi and Haddad 2020; Tranter et al. 2008) and shredded tyres (Gharavi et al. 2023; Mazumder et al. 2018; Shariatmadari et al. 2018) are the most successful and widely adopted options. Recycled waste glass (RWG) is another sustainable material for columnar inclusions with similar material properties to natural aggregates (Kazmi et al. 2024; Premathilaka et al. 2024). However, the bulging failure of columns in weak soft ground conditions is a problem when unbound materials such as recycled aggregates, shredded tyres and RWG aggregates are used. The geopolymer-bound recycled waste glass composite (GRWGC) developed by Premathilaka et al. (2026) provides a successful solution to address this issue in columns with above mentioned unbound materials. The novel composite utilises a RWG-based geopolymer, which enhances the column stiffness by improving interparticle bonding between RWG aggregates for better structural performance (Premathilaka and Liyanapathirana 2026; Premathilaka et al. 2026).

Numerical modelling using the finite element method (FEM) is the most commonly practised, flexible and time-saving method of analysing the behaviour of column-supported embankments. Linear elastic perfectly plastic Mohr-Coulomb constitutive model with a high friction angle and a low cohesion is commonly used to simulate the behaviour of unbound stone columns. However, the consolidated drained (CD) triaxial results of the proposed GRWGC material exhibit post-peak strain softening behaviour with significant dilation, deviating from the perfectly plastic behaviour typically assumed

in modelling stone columns (Premathilaka and Liyanapathirana 2026). Capturing the post-peak strain-softening behaviour in FEM modelling is critical to study the post-yield plastic behaviour of the new composite, especially when investigating the embankment behaviour in the ultimate limit state. Hence, it is crucial to develop a well-representative and stable constitutive model to be used in FEM analysis of columns with GRWGC.

This paper introduces a modified elastoplastic Mohr-Coulomb constitutive model that accounts for the post-peak strain softening behaviour of the proposed GRWGC material for stone columns. The stress-strain responses obtained for the GRWGC from CD triaxial tests were used to validate the modified constitutive model with a two-dimensional (2D) axisymmetric triaxial test simulated in the ABAQUS/Standard finite element Software. A well-documented case study of a load test carried out on soft ground improved with stone columns at a stockyard of ThyssenKrupp Company (TKCSA), located in Itaguaí District, Rio de Janeiro, Brazil (Almeida et al. 2014; Almeida et al. 2019) was studied with a three-dimensional (3D) finite element model. A comparison of field-measured settlements, lateral deformations and excess porewater pressures developed at different locations of the improved ground was conducted with the FEM results to validate the numerical model. The effectiveness of the proposed material was demonstrated using the same case study with GRWGC columns of varying column diameters. Finally, a parametric study was conducted on a hypothetical column-supported embankment with proposed GRWGC columns. Here, the effects of five design parameters: (i) column spacing, (ii) column diameter, (iii) tensile stiffness of the geogrid, (iv) fill height and (v) rate of embankment construction on six parameters governing the overall embankment performance: (i) stress concentration ratio (SCR), (ii) arching ratio (AR), (iii) maximum settlement (iv) differential settlement at the embankment base level, (v) lateral displacement at the embankment toe and (vi) maximum tension of the geogrid, were investigated to emphasise the influence of each design parameter on the performance of the proposed ground improvement method as a design guideline. The SCR was calculated as the ratio of the average vertical stress on a column to that applied on the effective area of foundation soil surrounding a column. The AR was determined as the ratio of the average vertical stress on the geogrid at the centre region of a 2×2 column arrangement to the total stress due to embankment weight (γH), where γ is the unit weight of the fill material and H is the fill height (Han and Gabr 2002).

2. Modelling the strain-softening behaviour of the proposed GRWGC material

2.1 Development of the constitutive model

Strain-softening behaviour is commonly observed in stiff clays, soft rocks, naturally structured soils and cemented soils, all of which are frequently encountered in geotechnical applications. There are constitutive models to simulate the strain-softening behaviour based on damage mechanics due to crack evolution in rock (Shen et al. 2019) and elasto-plastic

behaviour combined with a hardening parameter, which depends on the plastic work (Guo and Li 2008). The numerical studies on circular tunnels (Wang et al. 2010), landslides (Troncone 2005), cut slopes in stiff clay (Potts et al. 1997), deep cement-mixed column-supported embankments (Wijerathna and Liyanapathirana 2021; Yapage et al. 2015) have successfully simulated the strain-softening behaviour of geomaterials. Potts et al. (1997), Yapage et al. (2015) and Wijerathna and Liyanapathirana (2021) incorporated softening behaviour into the Mohr-Coulomb model by decreasing the mobilised friction angle (φ_{mob}), dilation angle (ψ_{mob}) and cohesion (C_{mob}) with accumulated plastic deviatoric strains (ε_{dp}).

Triaxial test results of the new GRWGC showed a reduction in mobilised cohesion and dilation angle, with increasing mobilised friction angle during the post-peak softening phase (Premathilaka and Liyanapathirana 2026). These parameters stabilised at their respective residual values at the end of the softening phase as the material reached a perfectly plastic behaviour. Considering the varying rate of softening in the post-peak stress-strain behaviour of the GRWGC in the softening phase, an additional set of parameters was introduced at the intermediate plastic deviatoric strain ($\varepsilon_{dp,\ int}$) for friction angle (φ_{int}), dilation angle (ψ_{int}) and cohesion (C_{int}) in addition to the model parameters at peak state: plastic deviatoric strain ($\varepsilon_{dp,\ peak}$), friction angle (φ_{peak}), dilation angle (ψ_{peak}), cohesion (C_{peak}), and at residual state: plastic deviatoric strain ($\varepsilon_{dp,\ res}$), friction angle (φ_{res}), dilation angle (ψ_{res}), cohesion (C_{res}) as shown in Fig. 1. A user-defined field subroutine (USDFLD) was used in this study to incorporate the post-peak softening behaviour of the GRWGC into the ABAQUS/Standard finite element Software as a modification to the inbuilt Mohr-Coulomb model.

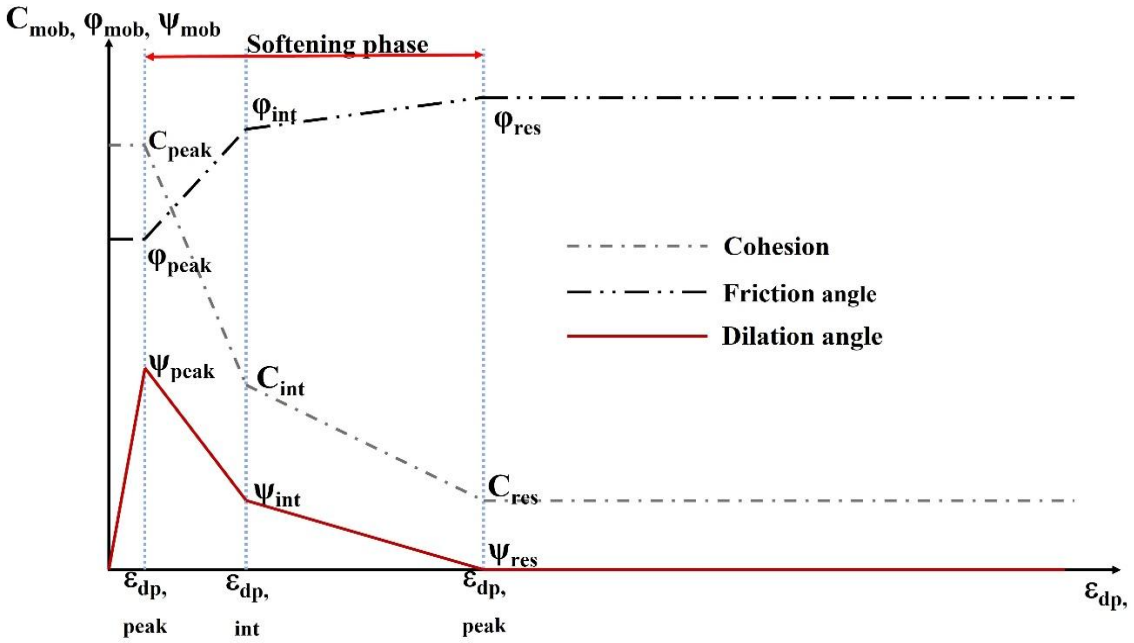


Fig. 1: Mobilised cohesion (C_{mob}), fiction (φ_{mob}) and dilation angles (ψ_{mob}) with plastic deviatoric strain (ε_{dp}) for GRWGC.

2.2 Validation of the constitutive model

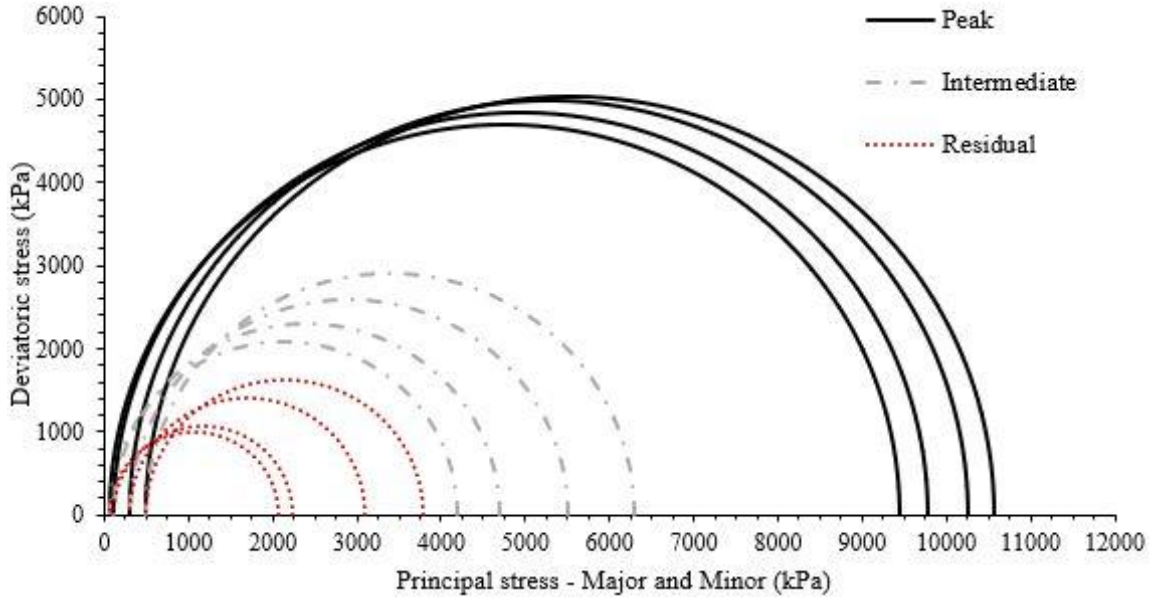


Fig.2: Mohr's stress circles at peak, intermediate and residual states.

The performance of the proposed constitutive model for the GRWGC should be validated before the numerical simulation of the embankment supported by GRWGC columns. The CD triaxial tests performed on GRWGC samples were simulated using the extended Mohr-Coulomb model described in the previous section. The drained fiction angle and cohesion at peak, intermediate (the point of inflection as shown in Fig. 1) and residual states were captured from the sets of Mohr's stress circles drawn as shown in Fig. 2, based on the CD triaxial experimental results. The dilation angles at each confining pressure were obtained from the volumetric strain variation with axial strain, and the elastic modulus of the GRWGC was calculated based on the stress-strain data (Premathilaka and Liyanapathirana 2026). The model parameters used for the validation process are tabulated in Table 1.

Table 1: The model parameters for GRWGC

E (MPa)	φ_{peak}	C_{peak} **(kPa)**	ψ_{peak}	$\varepsilon_{dp,\,peak}$	φ_{int}	C_{int} **(kPa)**	ψ_{int}	$\varepsilon_{dp,\,int}$	φ_{res}	C_{res} **(kPa)**	ψ_{res}	$\varepsilon_{dp,\,res}$
980.6	29.25°	2800	18.5-13.2°	0.00085	35.0°	1100	6.5-3.0°	0.004	36.13°	490	0	0.0146

Note: E – Elastic modulus

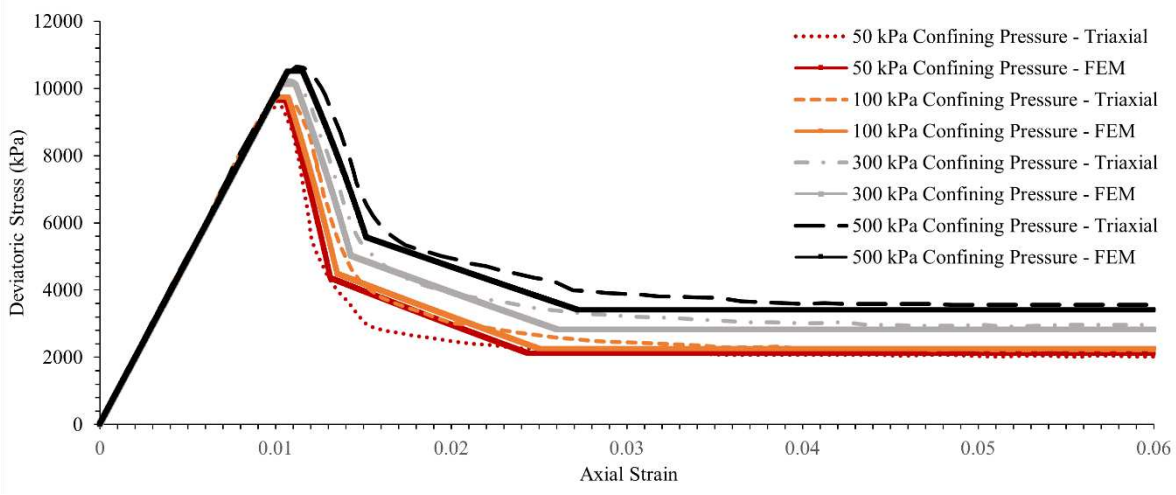


Fig. 3: Comparison of stress-strain behaviour of triaxial tests and FEM simulations

A 2D axisymmetric model of the cylindrical CD triaxial specimen measuring 50 mm in diameter and 100 mm in height was simulated considering the symmetry and drained behaviour. The GRWGC was modelled using 4-node axisymmetric quadrilateral elements with reduced integration and pore pressure degrees of freedom (CAX4RP). The stress-strain results of the simulation for four different confining pressures (50, 100, 300 and 500 kPa) were compared with the experiments (Premathilaka and Liyanapathirana 2026) as shown in Fig. 3. This comparison confirms the capacity of the proposed constitutive model to simulate the behaviour of GRWGC during the strain-softening phase successfully. It is important to note that the parameters used in this study are only valid for the material combination used to develop the GRWGC, as described by Premathilaka et al. (2026). The parameters need to be re-evaluated for different mix designs adopted for the composite, which consists of RWG aggregates, fine RWG powder, Sodium Hydroxide (NaOH) pellets, waste Aluminium (Al) foil and water.

3. Comparison of the performance of stone columns and GRWGC columns

3.1 General description of the case study

The case study is a load test carried out on soft ground improved with stone columns at a stockyard of ThyssenKrupp Company (TKCSA), located in Itaguaí District, Rio de Janeiro, Brazil (Almeida et al. 2014; Almeida et al. 2019). Cone penetration tests have been conducted after the installation of stone columns, which were used for the ground profiling. The top layer of the in-situ ground comprises a 6.05 m thick soft clay layer, which is overlain by a 2.6 m fill layer serving as a working platform. Below the soft clay layer, there are four sand and clay layers located alternatively, having thicknesses of 2.6 m, 2.95 m, 9.90 m and 3.40 m, respectively, followed by another sand layer as shown in Fig. 4. The water table was located at 0.8 m below the ground surface. Stone columns of 1 m diameter and 11.25 m length were

constructed in a 12 x 7 square grid, with a 1.85 m centre-to-centre spacing. The subsurface soil profile, pile arrangement, and field measuring instrument locations are shown in Fig. 4 and Fig. 5. There are eleven settlement plates (S) positioned at 0.5 m depth. Two inclinometers (I) are at 0.75 m and 6.05 m to the west of the loading area, each extending up to 23 m depth. There are nine vibrating wire piezometers (P) installed at 4 m, 4.5 m, 6 m (x2), 7 m, 7.5 m and 8.3 m depths. There are five magnetic extensometers (EX) placed at 6 m, 11 m, 14 m, 23.5 m and 27 m depths, and four earth pressure cells (EP) are placed at 4.5 m, 6 m, 7.5 m and 8.3 m depths. Steel rails were used to apply the surcharge loading, which is supported by a concrete slab with a 6.5 m x 6.5 m plan area. As shown in Fig. 5, the slab covered 16 stone columns in a 4 x 4 grid in the plan view. The concrete slab is placed on a 0.2 m thick gravel layer at the centre of the improved area, which acts as a drainage layer above the stone columns as shown in Fig. 4 and Fig. 5. The maximum surcharge of 183.6 kPa was applied on the 27th day of loading, and the loading-unloading sequence of the test area is shown in Fig. 6.

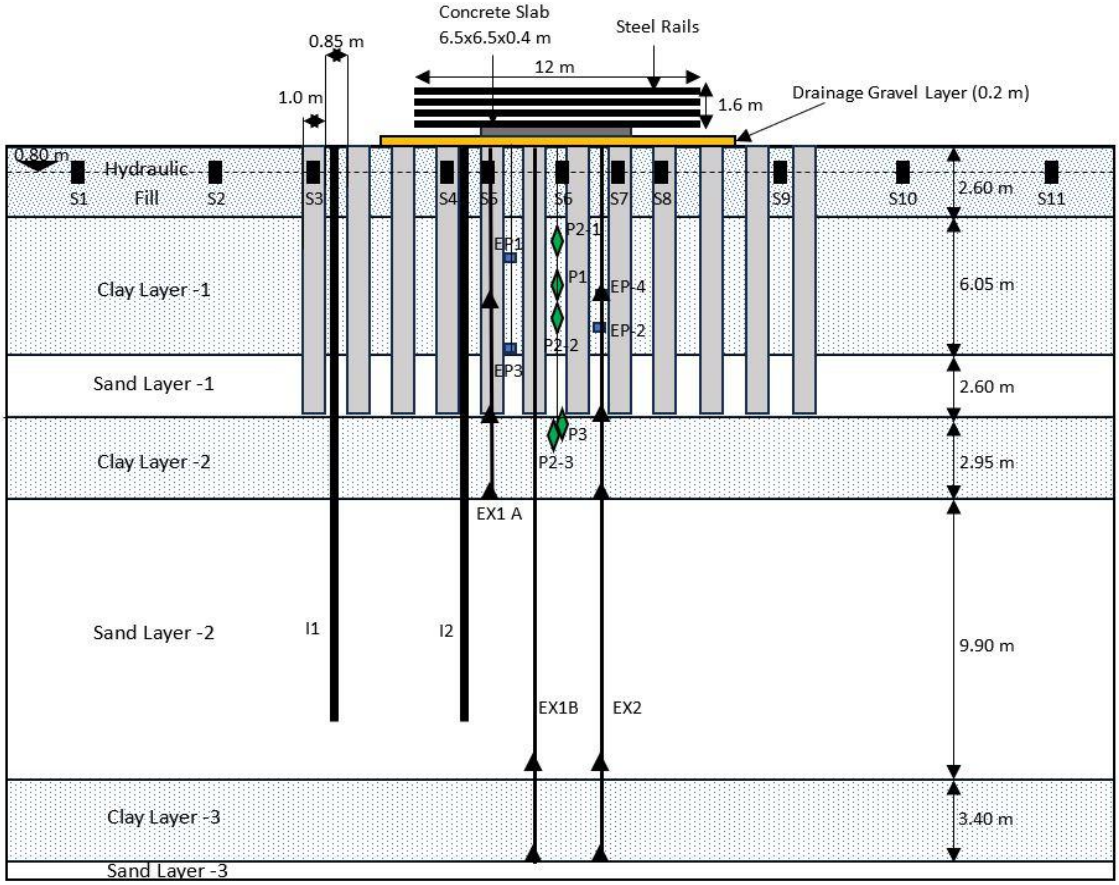


Fig. 4: Soil profile, column arrangement and instrumentation of the test area (Almeida et al. 2014).

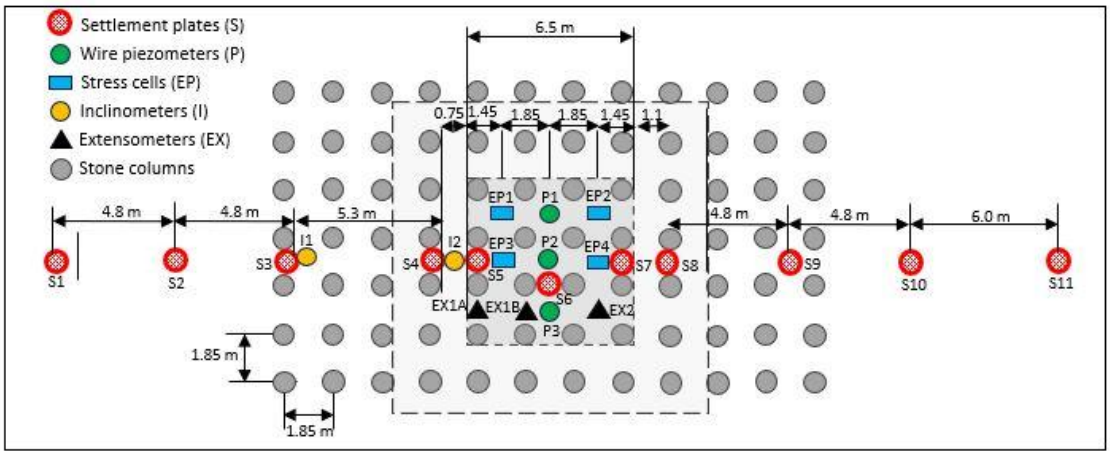


Fig. 5: Instrumentation and column layout - Plan view (Almeida et al. 2014).

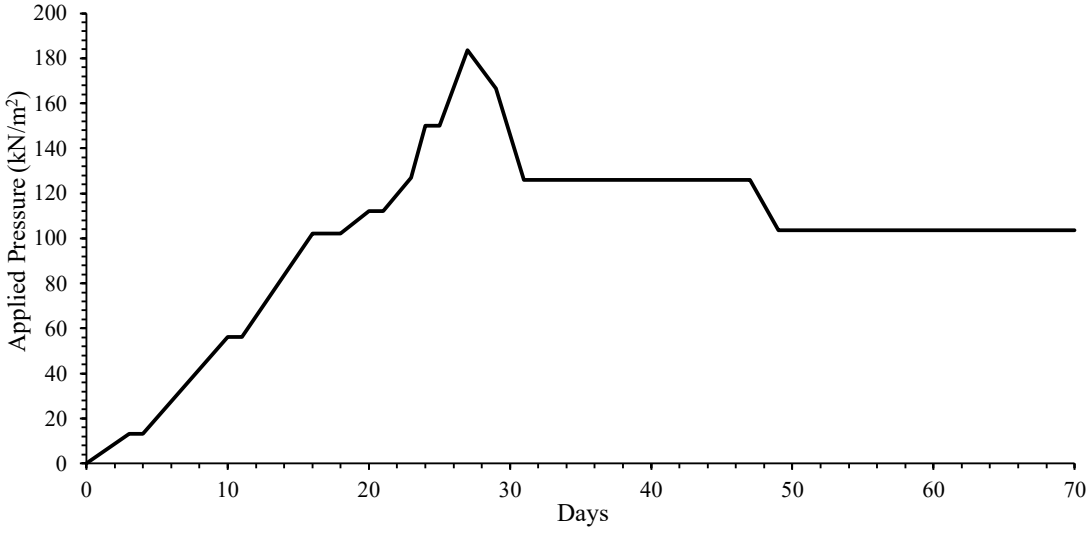


Fig.6: Loading sequence in the test area (Almeida et al. 2014).

3.2 Numerical model

3.2.1 Material models and parameters

The constitutive behaviour of the three clay layers was modelled using the modified Cam clay (MCC) model. The parameters, including the slope of the critical state line (M), the slope of the swell line (κ) and the slope of the virgin consolidation line (λ) required for the MCC model were derived from the material properties obtained from both field and laboratory test data reported by Almeida et al. (2014). All MCC material model parameters are summarised in Table 2. The Mohr-Coulomb (MC) model was used for all the coarse-grained materials, assuming linear elastic-perfectly plastic behaviour. The material properties of the stone columns, fill layer and three sand layers are summarised in Table 3. The concrete slab used as the loading platform was modelled using linear elastic behaviour, and the parameters are given in Table 4. The best-fit value for the lateral earth pressure coefficient (K_o) for the improved area was given as 1.25,

considering the disturbances caused by the installation process of stone columns (Almeida et al. 2014; Almeida et al. 2019). Hence, K_o of the fill layer was taken as 1.25 in this analysis.

Table 2: MCC model parameters for clay layers

Parameters (Units)	**Clay Layer-1**	**Clay Layer-2**	**Clay Layer-3**
Bulk unit weight, γ_b (kN/m^3)	13.4	16.0	15.6
Lateral earth pressure coefficient, K_o	0.6	0.60	0.60
The slope of the virgin consolidation line, λ	0.8348	0.4652	0.4348
The slope of the swell line, κ	0.1261	0.0565	0.0522
Stress ratio, M	0.984	0.984	0.984
Over-consolidated ratio (OCR)	1.08	1.08	1.08
Coefficient of horizontal permeability, k_h (m/day)	$7.9\text{x}10^{-5}$	$7.8\text{x}10^{-5}$	$1.4\text{x}10^{-4}$
Coefficient of vertical permeability, k_v (m/day)	$3.9\text{x}10^{-5}$	$3.9\text{x}10^{-5}$	$7.0\text{x}10^{-5}$
Initial void ratio, e_o	3.05	1.68	1.85

Table 3: MC model parameters for coarse-grained layers

Parameters (Units)	**Stone Column**	**Fill**	**Sand Layer-1**	**Sand Layer-2**	**Sand Layer-3**
Bulk unit weight, γ_b (kN/m^3)	20.0	18.0	18.0	18.0	18.0
Lateral earth pressure coefficient, K_o	0.35	1.25	0.5	0.5	0.5
Drained friction angle, φ (degrees)	40	30	30	30	30
Young's modulus, E' (MPa)	80	2	30	30	30
Poisson ratio, ν	0.3	0.3	0.3	0.3	0.3

Table 4: Parameters for the concrete slab

Material	**Bulk unit weight γ (kN/m^3)**	**Axial Stiffness EA (kN/m)**	**Flexural stiffness EI (kNm^2/m)**	**Poisson ratio ν**
Concrete slab	25	$1.2\text{x}10^7$	$1.6\text{x}10^5$	0.2

3.2.2 3D finite element model

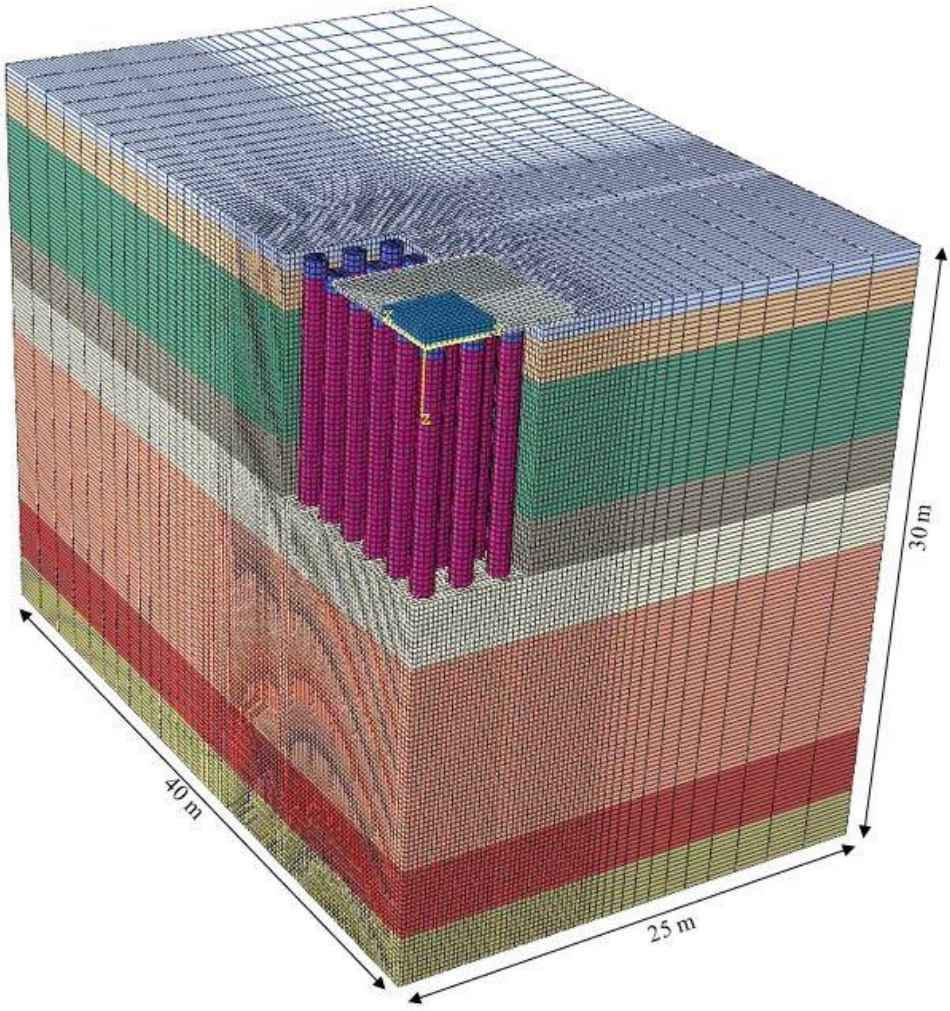


Fig. 7: Three-dimensional finite element model.

Fig. 7 shows the finite element model used to simulate the behaviour of the reinforced ground during the load test. Fully drained conditions were assumed for the hydraulic fill, gravel layer and the upper segment of the stone columns above the groundwater table, considering the high permeability of those materials. These sections and the concrete slab used as the loading platform were modelled with 20-node quadratic brick elements with reduced integration (C3D20R). The soil layers and the regions of stone columns below the water table were modelled using 20-node quadratic brick elements with reduced integration and pore pressure degrees of freedom at corner nodes (C3D20RP).

The loading platform was positioned asymmetrically along the xz-plane as column rows outside the loading area on the xz-plane differ on either side of the loading area by one to two rows. Hence, the centreline of the xz-plane was selected across the centre of the loading area. The part having a single pile row outside the loading area was considered in the finite element model, assuming the worst-case scenario. Also, considering the symmetry, only half of the profile on the yz-plane was included in the model. The bottom boundary of the model was placed at a depth of 30 m, which is 18.75 m

below the toe level of stone columns. A 40 m along the x-direction and a 25 m along the y-direction in the horizontal direction were considered in the finite element model to minimise the boundary effects on the key parameters involved in evaluating the performance. The bottom boundary on the xy-plane was fixed for the displacement in all three directions, and the boundaries along the centrelines in both the yz-plane and xz-plane were assigned symmetrical boundary conditions. The far boundary in the yz-plane was restrained in the x-direction, and similar boundary conditions were applied to the far boundary in the xz-plane by restraining it in the y-direction. All above five boundaries were set as impermeable, and the groundwater table at 0.8 m depth below the surface was set as a drainage boundary. A finer mesh was used in the reinforced area of the ground, including its vicinity, but beyond that region, the coarseness of the mesh was increased towards the outer boundaries of the domain to optimise the computational time while maintaining the accuracy of results, as shown in Fig. 7.

During the load test simulation, the loading was simulated as a variation of evenly distributed pressure applied on the concrete slab and controlled by an amplitude function varying with analysis time. The analysis started with the geostatic equilibrium step for the initial conditions of the ground reinforced with stone columns without any surcharge load. The loading sequence given in Fig. 6 was covered in seventeen steps, including seven loading, seven consolidating and three unloading steps, spanning over 70 days.

3.3 Numerical model validation

3.3.1 Settlements

The settlement measurements of plates positioned at S7 and S8, as shown in Fig. 5 covering the loading phase (35 days) of the test, were reported by Almeida et al. (2014). Fig. 8 shows the measured and numerically obtained settlements at S7 and S8 against time, which shows an excellent agreement. The maximum settlements measured by plates S7 and S8 were 98.4 cm and 13.2 cm, respectively, and the predicted settlements at these locations are 100.2 cm and 12.6 cm. The results confirm the successful simulation of the actual reinforced ground in the finite element simulation.

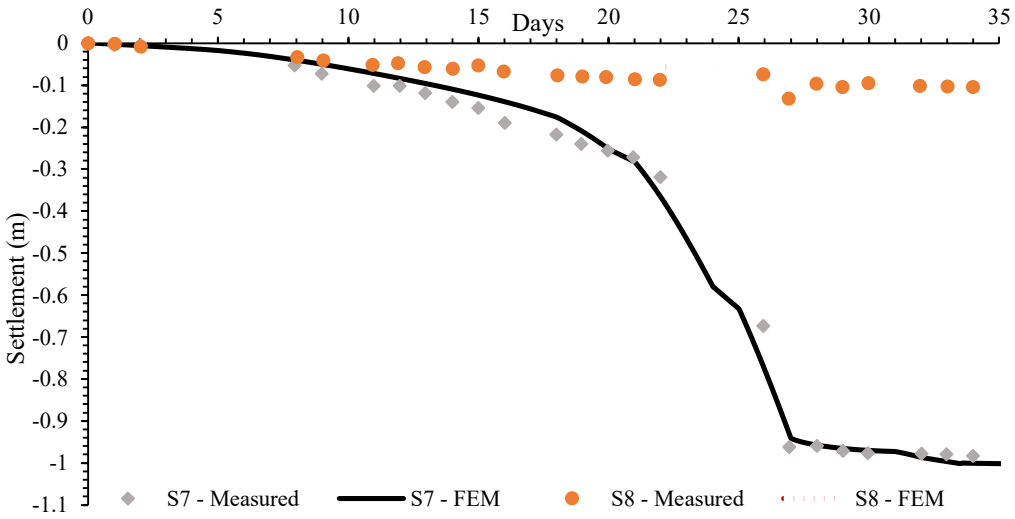


Fig. 8: Settlement variation at S7 and S8.

3.3.2 Lateral displacements

The lateral displacements measured along the inclinometer I2 at 3.5 m and 8.0 m depths during the loading phase of the test are compared with those computed with numerical modelling. Both measured and estimated values exhibit a good agreement, as shown in Fig. 9. The maximum lateral displacement measured at 3.5 m and 8.0 m depths were 32.6 cm and 4.6 cm, respectively, and the predicted lateral displacements of these locations are 29.9 cm and 6.2 cm. The comparison of the measured and computed lateral displacement values further confirms the realistic simulation of the actual site conditions.

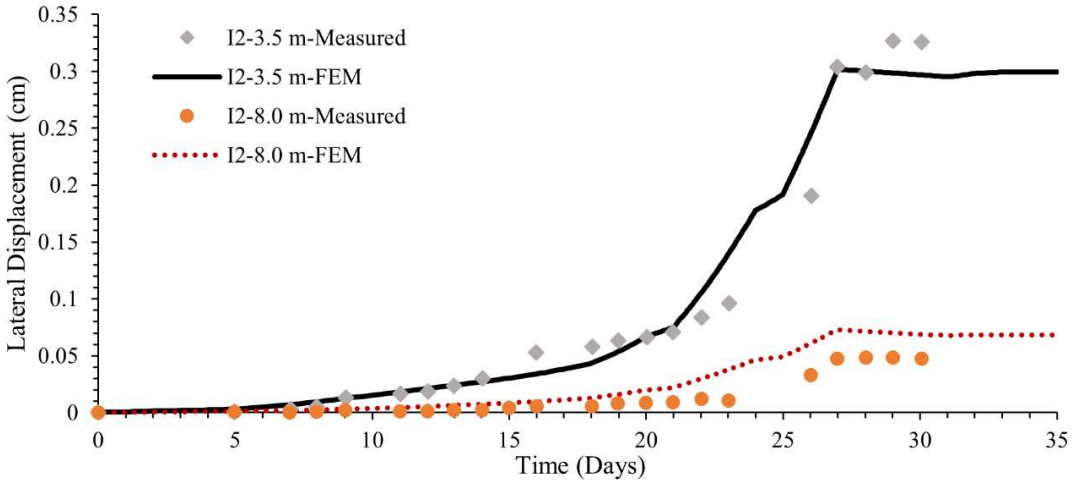


Fig. 9: Lateral deformation variations at 3.5 m and 8.0 m depths along I2.

3.3.1 Excess pore pressure

The excess pore pressure variation measured due to the loading using the piezometers P2-1, P1 and P2-2 located at depths of 4.0 m, 6.0 m and 7.0 m is compared with the simulation as shown in Fig. 10. The simulated variations of all three excess pore pressures follow the trend observed in the field measurements. The simulated variation of excess pore pressure at piezometer P2-1 (at 4.0 m depth) was slightly overestimated compared to the field measurement. However, significantly lower pore pressure increases were recorded at piezometers P1 (6.0 m depth) and P2-2 (7.0 m depth) in the field, compared to the numerical simulation. The overestimation of excess pore pressures by the numerical simulation may be attributed to permeability variations along the clay layer in the field, which were not accounted for in the numerical model due to limitations in the available data. These permeability variations may have resulted from disturbances that occurred in soil layers during the stone column installation process.

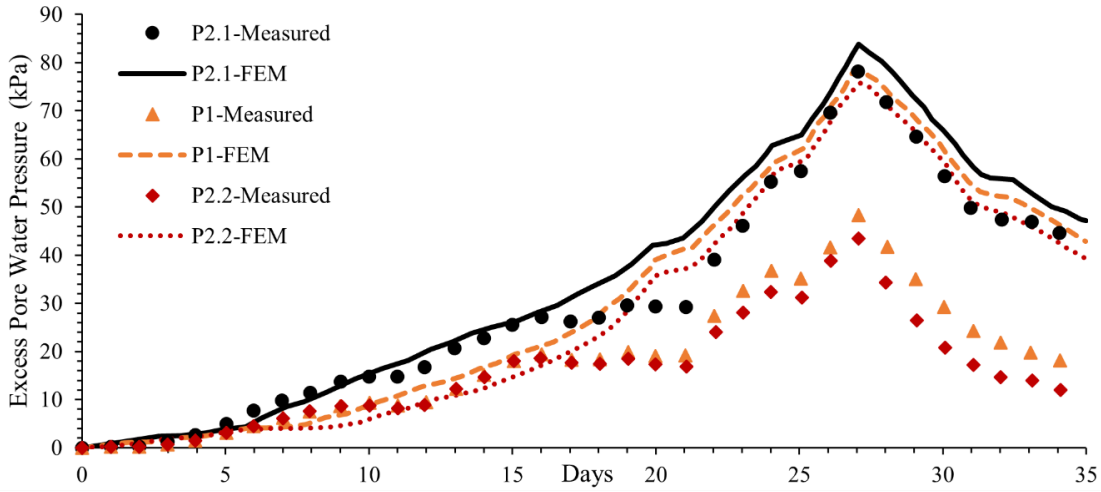


Fig. 10: Excess pore pressure variations at P2-1 (4.0 m), P1 (6.0 m) and P2-2 (7.9 m)

3.4 Performance comparison of stone columns and GRWGC columns

3.4.1 Background and model development

This section investigates the performance of the proposed GRWGC columns in ground improvement. The same case study used in section 3.3 with stone columns is used for the performance evaluation. The high stiffness of GRWGC, with an elastic modulus of 980.6 MPa, makes the composite material-based columns act as rigid columns, unlike traditional stone columns with an elastic modulus of 80 MPa. This high stiffness of GRWGC resolves the bulging failure issue, which is the primary drawback of stone columns in soft ground conditions. Also, the proposed new composite material mitigates the environmental and social impacts of natural aggregate production while offering a sustainable solution for repurposing glass and Al waste in solid waste management (Premathilaka et al. 2024).

The same material models used in the case study in section 3.3 were used for the soil layers in this section. The GRWGC columns were simulated using the extended Mohr-Coulomb material model proposed in Section 2, which is capable of capturing the strain-softening behaviour of GRWGC columns. The USDFLD subroutine was used as described in section 2 with the same model parameters to incorporate the strain-softening behaviour. The performance of reinforced ground was evaluated by applying the same loading sequence, as shown in Fig. 6 when the ground was improved with two column types explained earlier with different geometries.

The stiffer GRWGC columns replaced the stone columns discussed in the case study in section 3.3 with similar dimensions (1 m diameter, 11.25 m long) to compare the performance in this numerical analysis. The analysis was aborted after 25.9 days of loading. The settlements from the finite element analysis at S7 and S8 after 25.9 days were 0.138 m and 0.042 m, respectively, representing reductions of 85.1% and 60.4% compared to the case study with stone columns after the same duration. After 25.9 days, the maximum load applied on the top of a GRWGC column was 579.8 kN, with 316.91 kN (54% of the top load) transferred to the column toe. These values were significantly higher than those observed for unbound stone columns, where the top and toe loads were 407.6 kN and 56.4 kN, respectively, transferring only 14.0% of the load to the toe due to bulging. However, the additional load at the toe of the GRWGC columns exceeded the bearing capacity of Clay Layer 2, leading to convergence issues in the analysis. To address this issue, all GRWGC columns in the numerical analysis were extended by 2.95 m, passing through Clay Layer 2, with their toes positioned on the 9.9 m thick Sand Layer 2, which has a higher bearing capacity. To maintain compatibility, stone columns were also positioned at the same level in this section for the performance evaluation.

The column extension consumes 2.32 m^3 of additional materials per 1 m diameter column used in the case study but was offset by reducing the column diameter. The performance of the GRWGC columns was evaluated by comparing them to the 1 m diameter stone columns (SC-1D) in the case study. Three GRWGC column diameters of 1 m, 0.5 m and 0.25 m were denoted by CM-1D, CM-0.5D and CM-0.25D, respectively. The reduced diameters of 0.5 m and 0.25 m lowered material consumption per column by 6.05 m^3 and 8.14 m^3, respectively, for an 11.25 m long column.

3.4.1 Settlements

The settlement variations for the four cases; i) SC-1D, ii) CM-1D, iii) CM-0.5D and iv) CM-0.25D at points S7 and S8 are shown in Fig. 11(a) and Fig. 11(b), respectively. The performance of stone columns improved due to their positioning on Sand Layer 2, which provided additional end-bearing support compared to positioning them on Clay Layer 2. The replacement of column material with the GRWGC has reduced the settlements significantly, as shown in Table 5. These settlements show the advantage of using the proposed GRWGC material in ground improvement applications. The high

stiffness of GRWGC columns prevented them from bulging and buckling experienced by traditional stone columns, as shown in Fig. 12. The stiffer GRWGC columns directly transferred a significant portion of the load to the deeper, stronger Sand Layer 2, as shown in Table 5. This has reduced the percentage of load transfer to the soft clay layers and reduced both settlements as well as differential settlements of the improved ground. The high load-carrying capacity of GRWGC columns facilitates further optimisation of the ground improvement method by reducing the column diameter and spacing.

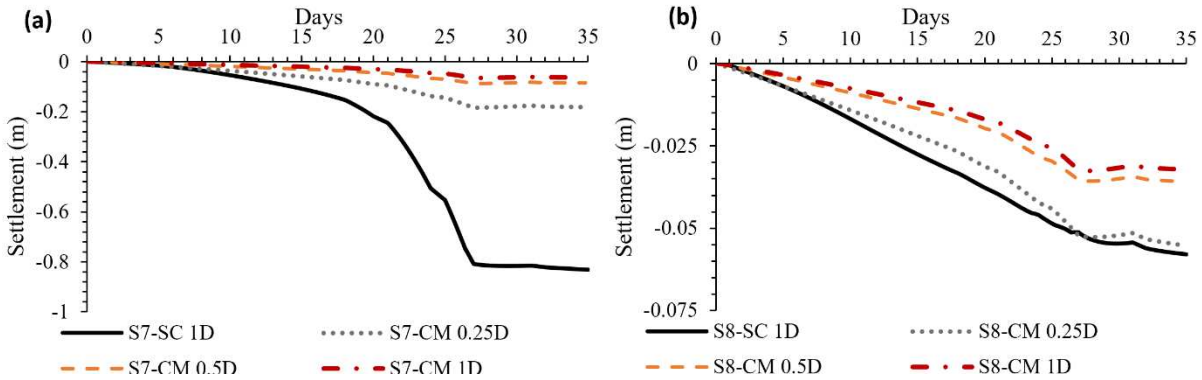


Fig. 11: Settlement variation of ground supported by different pile types/ sizes at (a) S7 and (b) S8

Table 5: Summary of settlements at S7 and S8 and maximum loads at the column top and the toe from column materials and geometries.

Parameter	SC-1D	CM-1D	CM-0.5D	CM-0.25D
Max. settlement at S7 (m)	0.831	0.063	0.085	0.182
Max. settlement at S8 (m)	0.058	0.032	0.036	0.055
Settlement reduction at S7 (%)*	-	92.4	89.8	78.1
Settlement reduction at S8 (%)*	-	44.8	37.9	5.2
Max. load at the column top (kN)	428.1	719.3	494.6	324.4
Max. load at the column toe (kN)	136.3	490.2	299.9	156.7

** Settlement reduction as a percentage of the settlement of 1 m diameter stone columns with the same column length*

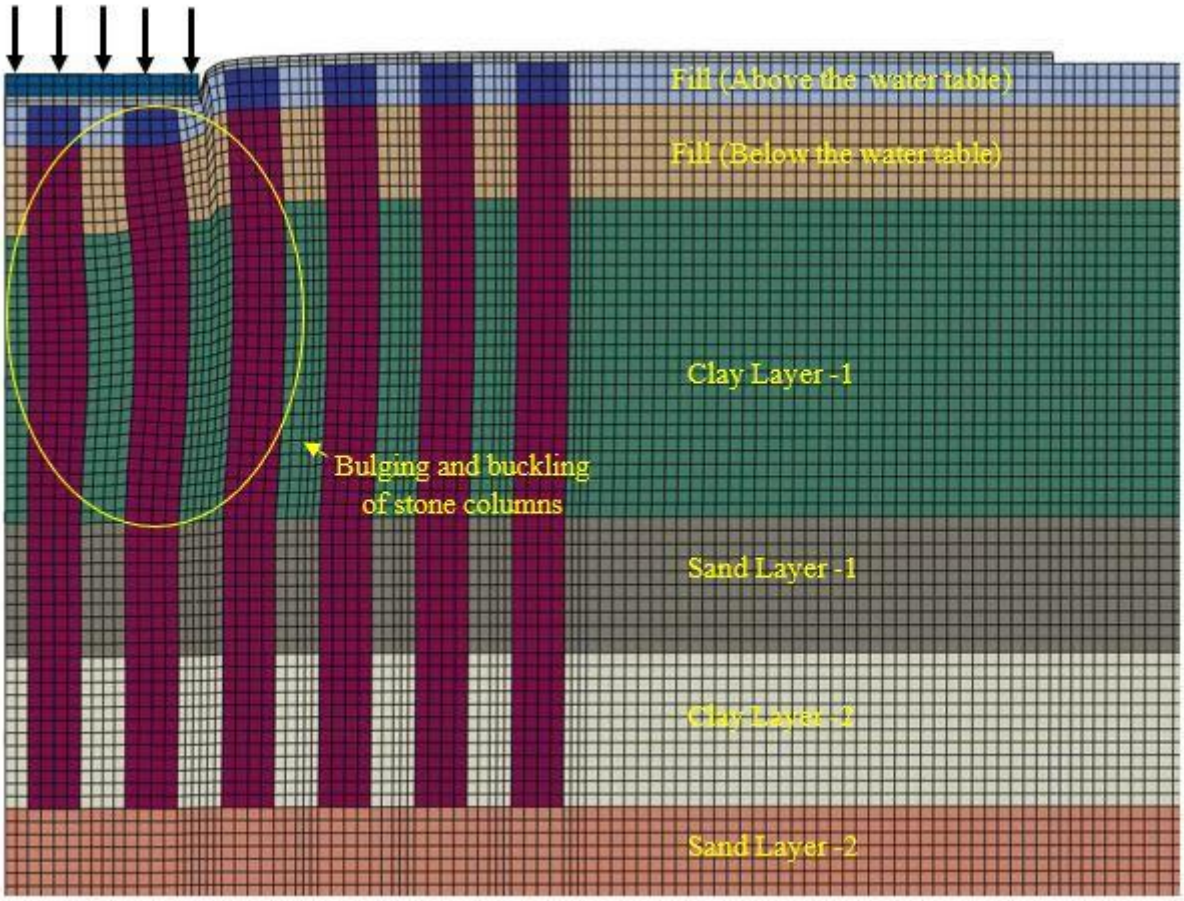


Fig. 12: Bulging and buckling of stone columns for case SC-1D

3.4.2 Lateral displacements

The variation of lateral displacements along the depth for the four cases SC-1D, CM-1D, CM-0.5D and CM-0.25D along the line of the inclinometer I2 are shown in Fig. 13. The observed maximum lateral displacements of cases SC-1D, CM-1D, CM-0.5D and CM-0.25D were observed at the depths of 4.36 m, 2.60 m, 2.85 m and 3.01 m, respectively. A maximum lateral displacement of 0.23 m was observed in the numerical analysis for case SC-1D (stone column improved ground). The replacement of the stone column material with GRWGC has significantly reduced the lateral displacements of the improved ground. The numerical results for the 1 m diameter GRWGC column (CM-1D) improved ground showed a negligible maximum lateral displacement of $6x10^{-3}$ m at the depth of 2.60 m. The GRWGC columns with diameters of 0.5 m and 0.25 m also showed significantly reduced lateral displacements. The reduction in the maximum lateral displacement of the improved ground with CM-0.5D and CM-0.25D, compared to 1 m diameter stone columns with the same column length, was 93.9% and 80.1%, respectively. The lateral displacement in the rigid column-improved ground is primarily influenced by the load applied to the foundation soil (Han 2015). The high stiffness of the GRWGC columns minimises the load applied to the foundation soil, as columns bear the majority of the load, as explained in Section 3.4.1.

The load carried by the columns increases with column diameter, as shown in Table 5, which results in a decrease in the maximum lateral displacement of the improved ground.

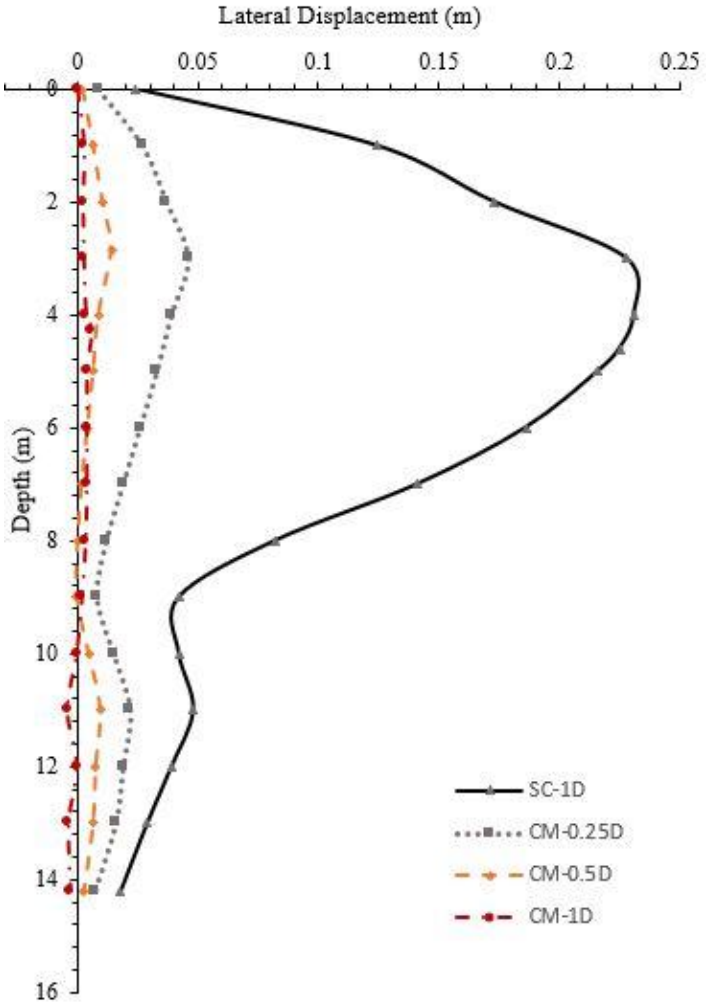


Fig. 13: Lateral displacement of ground improved with different column materials and geometries along the line of I2 inclinometer

4. Parametric study on GRWGC column-supported embankments

A comprehensive understanding of key design parameters is necessary for optimising both the short-term and long-term performance of improved ground, ensuring a successful and comprehensive column design. The numerical methods provide a flexible, time-saving and cost-effective option to achieve the optimum design parameters to maximise the performance of the improved ground. The key design parameters relevant to column-based ground improvement methods are: (i) column spacing, (ii) column diameter, (iii) tensile stiffness of the geogrid, (iv) embankment height and (v) embankment construction rate. The primary performance evaluation parameters are: (i) SCR, (ii) AR, (iii) maximum total settlements, (iv) maximum differential settlements, (v) lateral displacement at the embankment toe and (vi) maximum

tension in the geogrid. Therefore, finite element simulations were conducted to evaluate the influence of key design parameters on the embankment performance, which was quantified using the primary performance evaluation parameters. Results at the end of the embankment construction were referred for the short-term performance evaluation and 10 years after the embankment construction was considered for the long-term performance evaluation. Four different values were considered for every design parameter, and they were summarised in Table 6, with the baseline design parameters highlighted in bold font.

Table 6: Different design parameter combinations used in the parametric study

Item	Design parameter	Parameter combinations			
Column	Spacing (m)	1.5	**2.0**	2.5	3.0
	Diameter (m)	0.25	0.50	**0.75**	1.00
Geogrid	Tensile stiffness (kN/m)	50	250	**1250**	5000
Embankment Fill	Height (m)	1.2	2.4	**3.6**	4.5
	Construction rate (m/day)	0.025	**0.05**	0.1	0.2

4.1 Details of the hypothetical column-supported embankment

A hypothetical embankment, 40 m wide, 3.6 m in height, with a 1V:2H side slope, was used in this parametric study. A 0.5 m-thick gravel layer was placed at the bottom of the embankment, with a 4 mm-thick geogrid placed in the middle of the gravel layer. A ground profile consisting of a sand layer overlain by a 14 m-thick, soft clay layer was considered. GRWGC columns in a square pattern were positioned on the sand layer passing through the soft clay layer. The groundwater table was assumed to be at the ground surface. The properties of the soft clay layer and the sand layer were considered the same as those for the Clay Layer 2 (Table 2), except for the over-consolidation ratio, which was taken as 1.5. The properties for the Sand Layer 2 (Table 3) of the case study in Section 3 and the GRWGC properties are the same as those given in Table 1. The tensile stiffness of the geogrid was varied as shown in Table 6, and properties of the gravel and embankment layers used in this parametric study are given in Table 7.

Table 7: Material properties for gravel and the embankment fill

Material	Bulk density γ (kN/m^3)	Elastic modulus E (MPa)	Poisson ratio ν	Friction angle θ (degrees)	Cohesion c (kPa)
Gravel	18.5	30	0.3	40	10
Embankment fill	18.5	20	0.3	30	10

4.2 3D finite element modelling

A finite element model for the column-supported embankment system was developed in ABAQUS/Standard finite element modelling software, using the same method, validated in Section 3. Fully drained conditions were assumed for the embankment fill and the gravel layer located above the groundwater table, considering the high permeability of those materials. These sections were modelled using 20-node quadratic brick elements with reduced integration (C3D20R). The subsurface soil layers and the GRWGC columns below the water table were modelled with 20-node quadratic brick elements with reduced integration and pore pressure degrees of freedom at corner nodes (C3D20RP). The geogrid was modelled with an 8-node quadrilateral membrane element with reduced integration (M3D8R).

Considering the geometric symmetry of the problem, only half of the embankment was modelled in the x-direction. A complete soil depth of 30 m was considered in the model. GRWGC column toes were placed 16 m away from the bottom boundary to avoid any influence from boundary effects on the embankment performance. The vertical boundary was placed 60 m away from the centre line of the embankment, which is three times the width of the embankment. Half of the pile spacing from the centre of the pile was selected to choose the model width in the y-direction.

The bottom boundary on the xy-plane was fixed in all three directions for displacements, and the boundary along the centreline on the yz-plane was assigned a symmetrical boundary condition. The two vertical boundaries on the xz-plane were restricted against any horizontal movements in the y-direction. The vertical boundary in the yz-plane away from the centre line was restrained in the x-direction. All external boundaries were set as impermeable except the groundwater table on the ground surface, which was assigned a zero pore pressure boundary. A finer mesh was used in the reinforced area of the ground and its vicinity, as shown in Fig. 14, to optimise the computational time while enhancing the accuracy of the analysis.

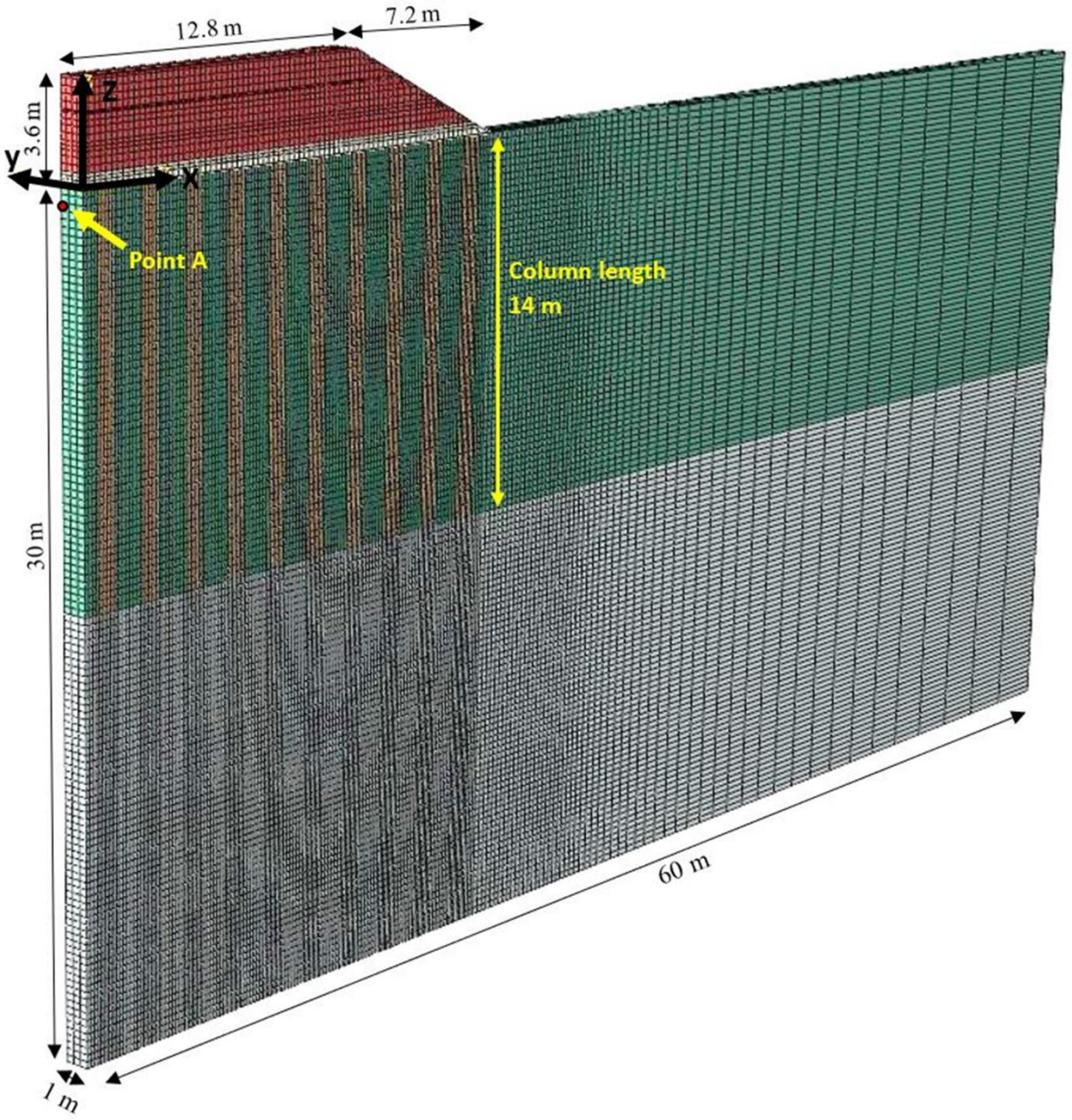


Fig. 14: 3D finite element model for the problem

4.3 Analysis of results

The results of the parametric study carried out with five varying design parameters for both short-term and long-term cases are discussed here. Six performance parameters were used in this study to evaluate the embankment performance: (i) SCR, (ii) AR, (iii) maximum settlement at the embankment base, (iv) maximum differential settlement at the embankment base, (v) lateral displacement at the embankment toe and (vi) maximum tension in the geogrid. Here, the graphical representations were used to illustrate the impact of each design parameter on the corresponding evaluation metrics.

The SCR values in all cases are significantly high due to the high stiffness of the columns relative to the soft clay layer. Consequently, a substantial portion of the embankment load is supported by the GRWGC columns, leading to higher SCR

values compared to unbound stone columns. This stress redistribution reduces the load applied on the foundation soil, thereby generating lower excess porewater pressure in the soft soil layer at the end of construction. Hence, post-consolidation settlements remain minimal, with limited parameter variations after 10 years. The maximum excess pore water pressure of 9.51 kPa was observed at the centre of the embankment, 0.7 m deep into the foundation soil (point A in Fig. 14) at the end of the embankment construction period for the baseline scenario of this parametric study.

4.3.1 Column Spacing

Column spacing is one of the key design parameters for column-based ground improvement methods, as it determines the number of columns required for the project. Even though smaller column spacing provides better reinforcement by increasing the area replacement ratios (ARR), it also raises project costs due to the greater number of columns required. Therefore, it is important to get the optimal column spacing as per the requirement for an efficient ground improvement design. Here, the column spacing varied between 1.5 m and 3.0 m, with corresponding ARRs in the range of 19.63% to 4.91%. A considerable increase in SCR and AR was observed with increasing column spacing, as shown in Fig. 15(a) and (b), due to the increase in vertical stresses applied on columns with increasing column spacing. Fig. 15(c) shows the maximum settlement measured at the centre of the embankment base (Fig. 14). With increasing column spacing, the maximum settlement at the embankment base shows an increase due to the increase in loads applied on foundation soil due to reduced ARR. Fig. 15(d) shows the maximum differential settlements against the column spacing observed at the embankment base. Differential settlements also show the same trend, similar to maximum settlements, with decreasing ARR. The differential settlements are about 50% of the maximum soil settlements for all cases, indicating significant column settlements during construction. The GRWGC columns used in this parametric study were not designed as end-bearing columns. They were positioned on a 16 m-thick sand layer located 14 m below the ground surface with a fixed boundary at the bottom of the finite element mesh. Therefore, differential settlements were low compared to ground improved with rigid end-bearing columns because end-bearing columns experience negligible settlements, resulting in higher differential settlements. A significant increase in the lateral deformation of the embankment toe could be observed with increasing column spacing. A 137% increase in the lateral movement was observed when column spacing varied from 1.5 m to 3.0 m, as shown in Fig. 15(e). This increase is due to the reduced resistance to lateral loading with increased column spacing. The maximum tension developed in the geogrid with the variation of column spacing as shown in Fig. 15(f). The increased load transfer to the geogrid due to wider column spacing explains the increase in maximum tension observed in the geogrid.

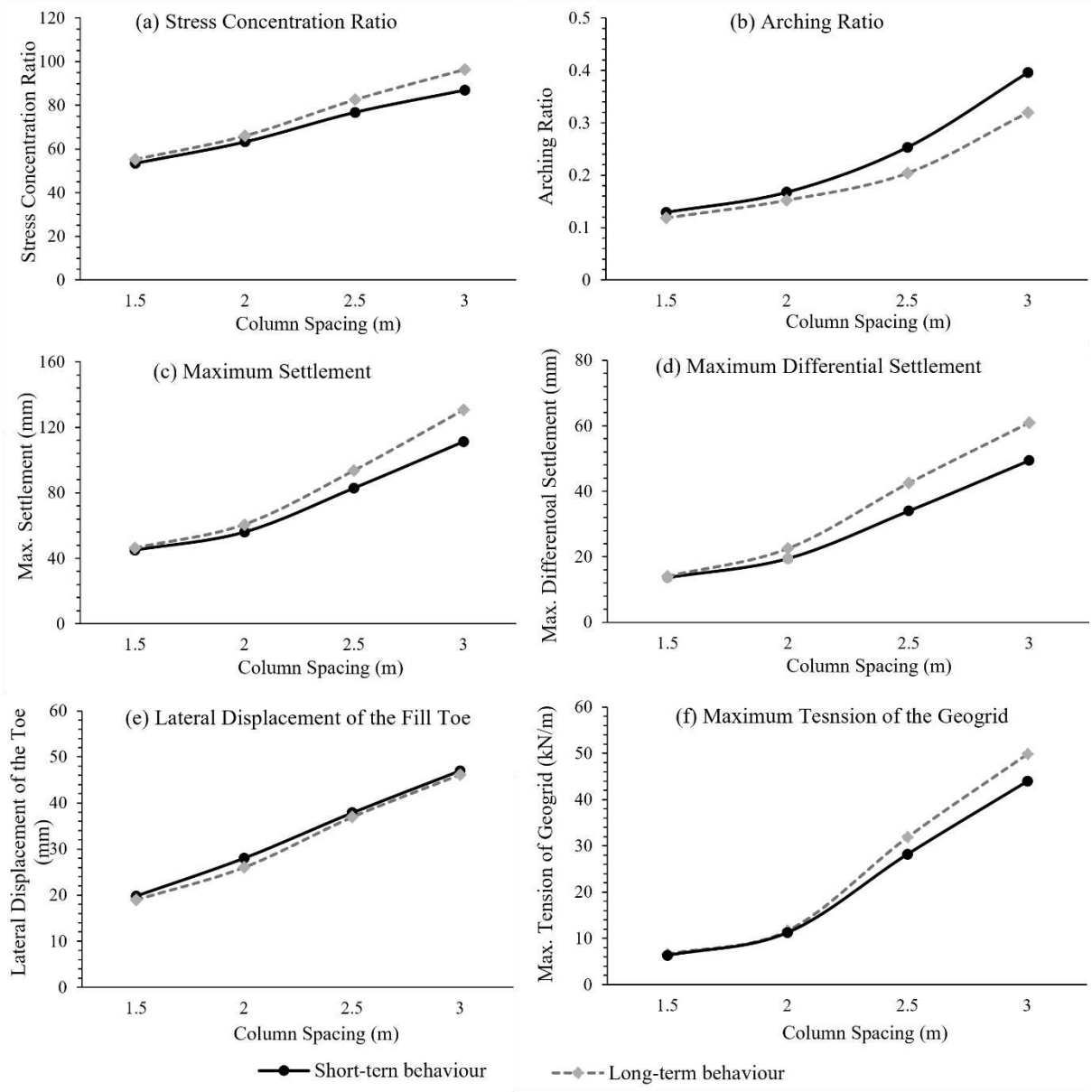


Fig. 15: Analysis summary of (a) SCR, (b) AR, (c) Maximum settlement, (d) Maximum differential settlement, (e) Lateral displacement of the toe and (f) Maximum tension of the geogrid against the column spacing

The small differences observed between short-term and long-term performance parameters suggest that the performance subsequent to embankment construction is not significant. The observed small differences post-construction are primarily driven by soil consolidation because the surrounding soil is highly compressible compared to rigid columns. According to Fig. 15(a), the increased SCR during consolidation suggests an increase in loads transferred to the columns. The loads transferred to the columns are governed by three factors: (i) soil arching within the embankment fill layers, (ii) vertical component of the geosynthetic tension due to membrane action, and (iii) shear stresses developed at the column–soft soil interface. As shown in Fig. 15(d) and (f), increased differential settlements (soil settles more than columns, indicating shear stress at the column-soil interface acting in the downward direction) and geosynthetic tension during consolidation increase the load transfer to columns over time, increasing the SCR and reducing the AR. This observation signifies

greater load transfer to the columns and a reduced load transfer to the geogrid as consolidation progresses. As shown in Fig. 15(c), consolidation increases maximum settlement in the foundation soil due to the increase in effective stresses in the soil with time. Since post-construction consolidation occurs only in the foundation soil, the increase in differential settlement is comparable in magnitude to the short- and long-term differences in maximum settlement. Lateral displacement at the embankment toe remains unchanged before and after consolidation, as lateral resistance is provided by the columns rather than the soil. Additionally, column strength remains constant post-construction since consolidation within the columns is not significant subsequent to construction. A comparison of Fig. 15(b), (c), and (f) indicates that the increase in geogrid tension is primarily due to foundation soil settlement rather than direct load transfer to the geogrid in the long-term case because the AR reduced during consolidation, indicating direct load transfer to geogrid reduced during consolidation. Notably, an AR of 0 represents full arching (where all embankment and traffic loads are transferred to the columns), while an AR of 1 indicates no arching (where the entire embankment load is carried by the foundation soil). Fig. 15(b) shows an AR of approximately 0.3, meaning 30% of the embankment load is supported by the foundation soil and geogrid. Thus, foundation soil settlement is the key factor influencing geogrid tension.

4.3.2 Column Diameter

Column diameter is another important design parameter considered in column-supported embankment design. The increasing column diameter enhances the ground reinforcement, providing stability to the improved ground. Conversely, the increasing column diameter directly impacts the project cost, as columns with larger diameters consume more materials. Therefore, it is important to get the optimal column diameter as per the requirement for an efficient ground improvement design. In this section, the influence of column diameter on embankment performance is investigated by varying diameters between 0.25 m and 1.0 m, which varied the ARR of the improved ground from 1.23% to 19.63%.

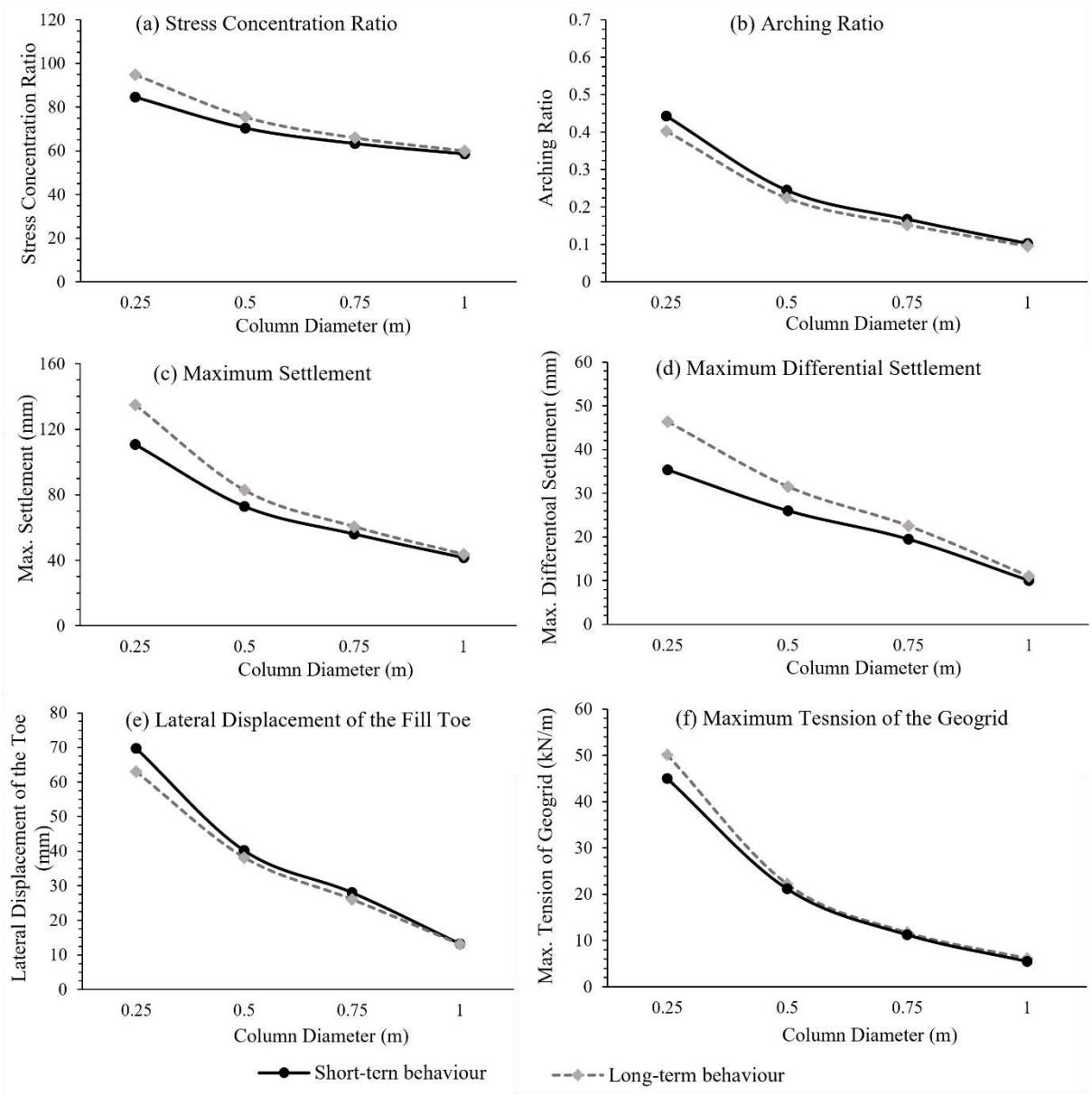


Fig. 16: Analysis summary of (a) SCR, (b) AR, (c) Maximum settlement, (d) Maximum differential settlement, (e) Lateral displacement of the toe and (f) Maximum tension of the geogrid against the column diameter

A considerable reduction in SCR was observed, as shown in Fig. 16(a), with the increasing column diameter, which increases the ARR, confirming a reduction in load transfer to columns. A similar trend was observed for AR in Fig. 16 (b), which indicates that a larger proportion of the embankment load was transferred to the columns with increasing diameter. This observation aligns with the findings of Borges and Marques (2011), who confirmed this behaviour using an axisymmetric finite element model. A pronounced decrease in settlements at the embankment base with the increasing column diameter is evident in Fig. 16(c). This reduction can be attributed to the decreasing vertical stress applied to the foundation soil as the ARR increases, which also influences the differential settlements, as shown in Fig. 16(d). A decreasing trend in lateral displacement of the embankment toe with increasing column diameter is observed in Fig. 16(e). The improved bending stiffness of large-diameter columns strengthens the ground's resistance to lateral deformations,

along with the reduction of active earth pressures acting on the columns with the increasing column diameters, subsequently reducing the lateral deformations of the embankment. The combined effect of reduced AR, settlements and lateral deformations minimises the development of tension in the geogrid as column diameter increases, as illustrated in Fig. 16 (f).

The SCR shown in Fig. 16(a) further increases with consolidation for long-term performance due to a further increase in load transfer to columns, while AR further decreases, as shown in Fig. 16(b), due to reduced load transfer to the foundation soil and geogrid. The observed SCR increase is mainly due to contributions from the membrane action of the geogrid and the shear stress acting at the soil-column interface. The highest difference between short- and long-term cases was demonstrated for the case with the smallest column diameter. For this case, the load transfer to soft foundation soil is the highest and hence, consolidation effects are more pronounced. Both maximum and differential settlements shown in Fig. 16(c) and (d) continue to increase in the long term due to the dissipation of excess pore water pressure generated in the soft soil layer during the construction stage, increasing effective stresses. A marginal reduction in long-term lateral displacement of the embankment shown in Fig. 16(e) was observed in comparison to the short-term results, showing increased lateral resistance with the progression of consolidation. The difference between short- and long-term lateral deformations is prominent for smaller column diameters, where more loads are transferred to foundation soil, increasing excess pore pressure generation in foundation soil. Therefore, consolidation effects are clearly visible when the column diameter decreases. The maximum tension in the geogrid slightly increases in the long term with the consolidation settlements, especially with small-diameter columns, as illustrated in Fig. 16(f). This is primarily due to the higher settlements shown in Fig. 16 (c), confirming the dependence of tension development on the settlement of the foundation soil more than the arching ratio, as explained earlier.

4.3.3 Tensile stiffness of the geogrid

The geogrid plays a critical role in optimising the modern column-supported embankments, significantly enhancing their overall performance. Its ability to improve the SCR of the reinforced ground by transferring a significant portion of loads applied on the geogrid to columns through tension via its membrane action is leveraged to optimise column arrangements and dimensions. The tensile stiffness of the geogrid is the governing design parameter that defines its performance, and it needs to be chosen considering the requirements of the application. In this study, the geogrid tensile stiffness was varied over a wide range between 50 kN/m and 5000 kN/m, providing sufficient information for practical applications.

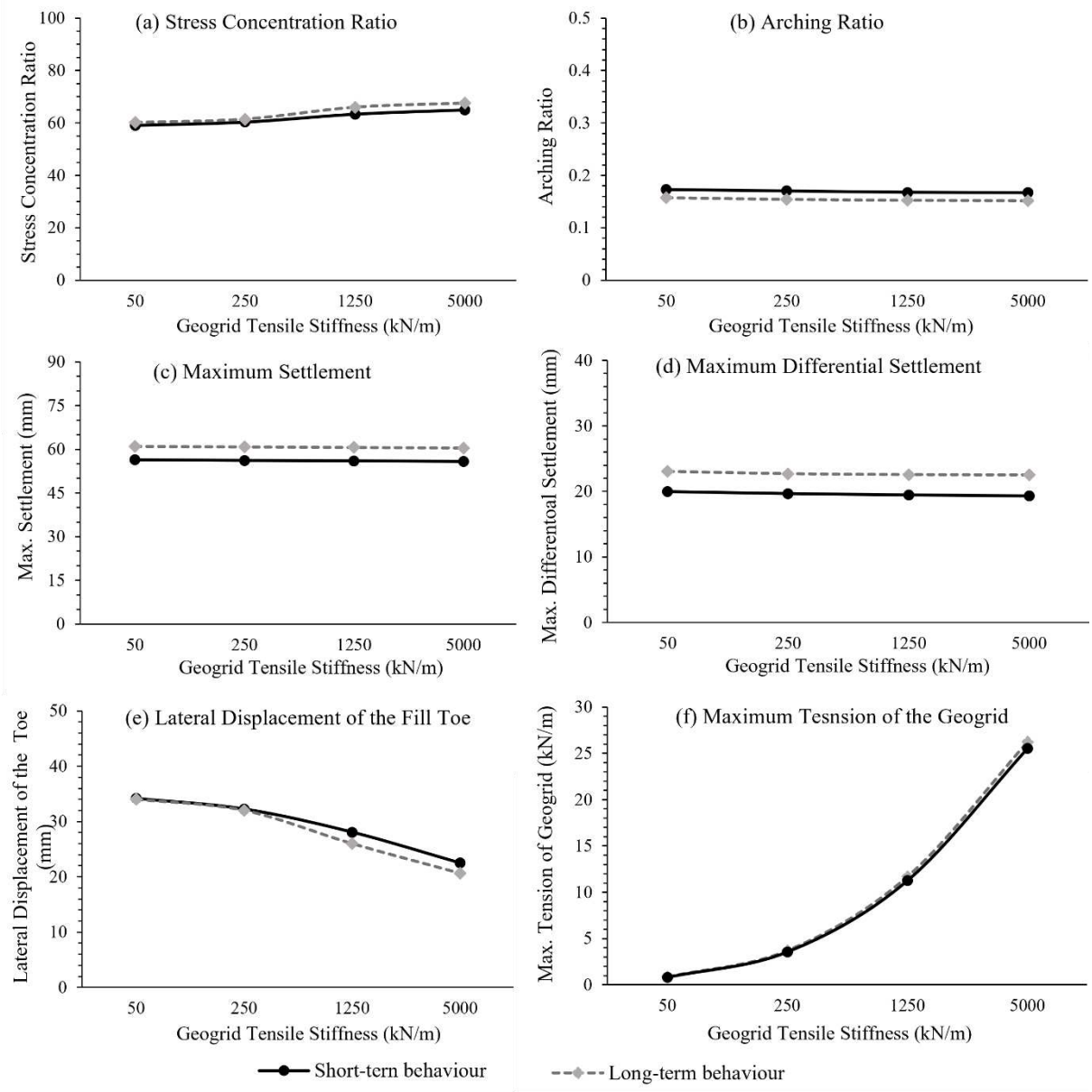


Fig. 17: Analysis summary of (a) SCR, (b) AR, (c) Maximum settlement, (d) Maximum differential settlement, (e) Lateral displacement of the toe and (f) Maximum tension of the geogrid against the tensile stiffness of the geogrid

Fig. 17(a), (b), (c) and (d) show that the increase in tensile stiffness of the geogrid does not have any significant influence on the load transfer to columns and the geogrid, max settlement and differential settlement, respectively. A considerable reduction in lateral displacement at the embankment toe, as shown in Fig. 17(e), was observed with increasing geogrid tensile stiffness. The lateral displacement decreased by 34% over the considered tensile stiffness range, as higher tensile stiffness enhances resistance to geogrid extension. Additionally, a significant increase in geogrid tension was observed with increasing tensile stiffness, as illustrated in Fig. 17(f). Since geogrid tension is defined as the product of strain and tensile stiffness, and strain remained consistent across all four cases in this parametric study, the increase in tensile stiffness from 50 kN/m to 5000 kN/m resulted in a directly proportional increase in geogrid tension. The influence of

geogrids on column-supported embankment performance may become more pronounced under higher surcharge loads during the serviceability stage.

In long-term cases, where consolidation effects govern the behaviour, load transfer to columns remained largely unchanged, as illustrated in Fig. 17 (a), while loads transferred to the geogrid decreased slightly. As a result, the long-term SCR remained similar to its short-term counterpart, whereas the arching ratio (AR) slightly decreased, as shown in Fig. 17(b). Due to the increase in effective stresses in the foundation soil during consolidation, maximum settlement also increased, leading to greater differential settlement of the improved ground, as shown in Fig. 17(c) and (d). However, no significant variation was observed between short-term and long-term behaviour in terms of lateral deformation at the embankment toe or geogrid tension, as shown in Fig. 17(e) and (f).

4.3.4 Embankment height

The impact of increasing load, represented by variations in embankment height ranging from 1.2 m to 4.5 m, on the evaluation parameters is analysed in this section. The increase in embankment height results in higher stresses applied on both columns and foundation soil. The distribution of stresses depends on the efficiency of soil arching and the performance of the geogrid. The SCR increased from 45.17 to 66.56 as the embankment height rose from 1.2 m to 4.5 m, as shown in Fig. 18(a). The improved soil arching action with increasing embankment height is the reason for the increasing SCR. In Fig. 18(b), a 14% reduction in AR is observed as the embankment height increases from 1.2 m to 2.4 m, indicating that the embankment reaches a sufficient height for the development of arching action, reducing load transfer to the geogrid.

A marked increase in the maximum settlement and maximum differential settlement at the embankment base level was observed, as shown in Fig. 18(c) and Fig. 18(d), respectively, with increasing embankment height. The increase in the overall load applied on foundation soil, corresponding to increasing embankment height, is the reason for increased settlements and differential settlements. Similarly, the lateral displacement of the embankment toe has also increased with increasing embankment height, as shown in Fig. 18(e), due to an increase in active lateral earth pressure with the increasing embankment height. The increased deformations due to increased embankment height caused the tension in the geogrid to rise, as shown in Fig. 18(f).

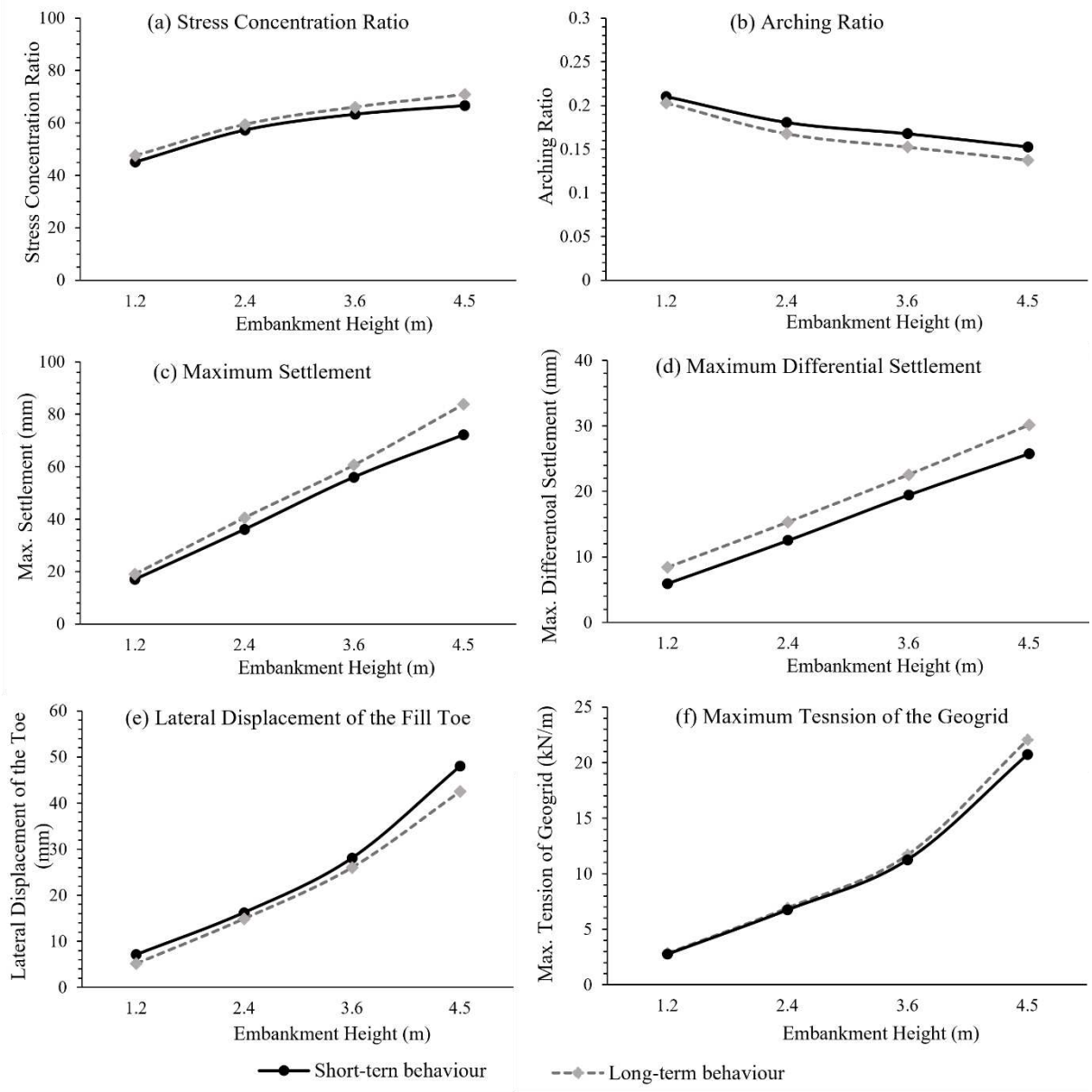


Fig. 18: Analysis summary of (a) SCR, (b) AR, (c) Maximum settlement, (d) Maximum differential settlement, (e) Lateral displacement of the toe and (f) Maximum tension of the geogrid against the embankment height

With the increase in embankment height, the difference between the short- and long-term behaviour of the embankment is marginal, indicating that the consolidation effects are not affecting the embankment performance. In the long term, consolidation of the foundation soil has increased load transfer to the columns, increasing SCR, as shown in Fig. 18 (a). Hence, the AR, which defines loads transferred to the geogrid, decreased as shown in Fig. 18 (b). Both maximum and differential settlements shown in Fig. 18 (c) and (d), respectively, increased during the consolidation of the ground due to increased effective stresses. Consolidation increases tension in the geogrid due to increased settlements of the foundation soil, as shown in Fig. 18(f). Due to increased membrane action and axial stresses developed in columns, lateral deformations of the improved ground decrease, as shown in Fig. 18(e).

4.3.5 Embankment construction rate

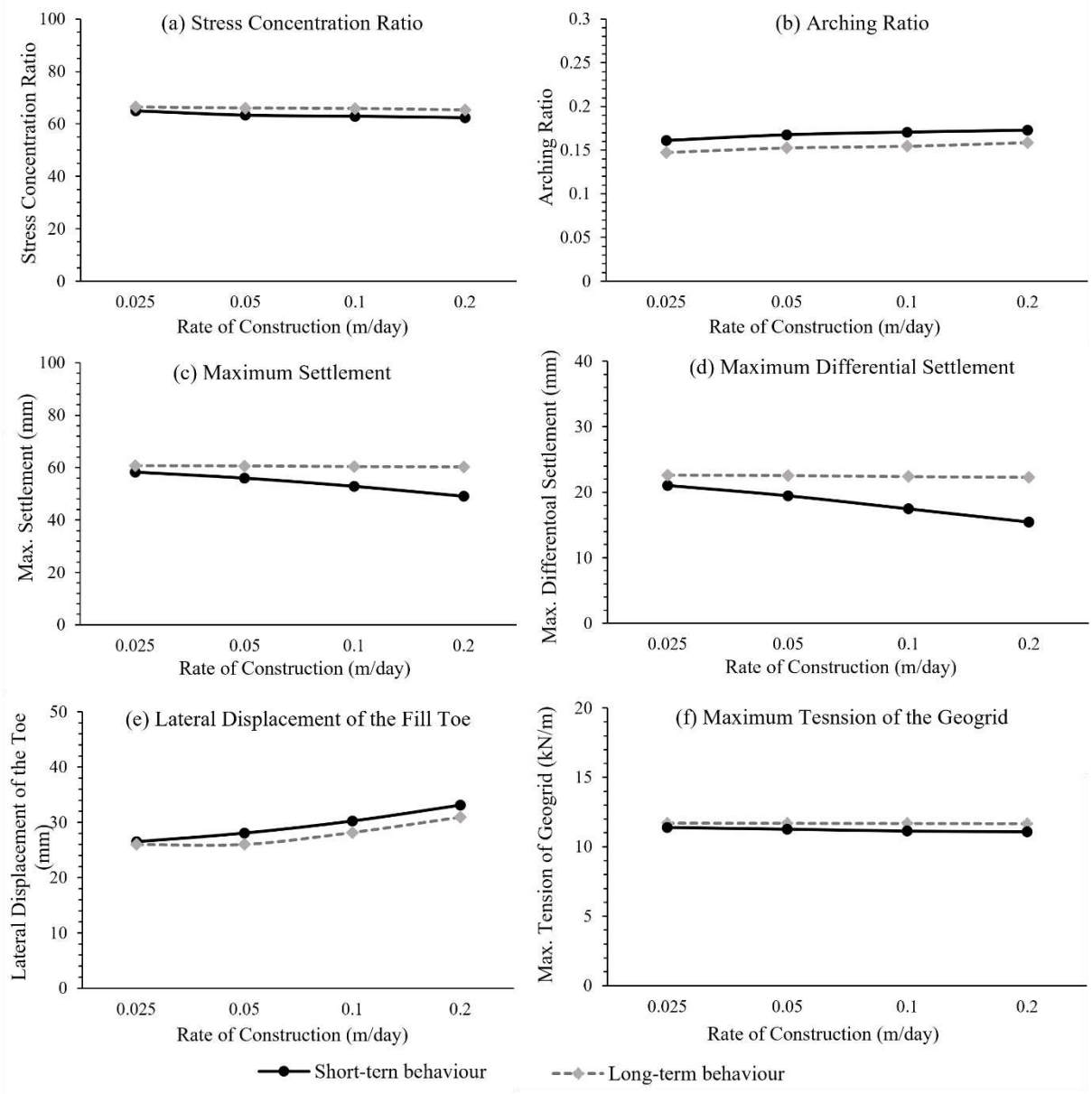


Fig. 19: Analysis summary of (a) SCR, (b) AR, (c) Maximum settlement, (d) Maximum differential settlement, (e) Lateral displacement at the toe and (f) Maximum tension of the geogrid against the embankment construction rate

The impact of the embankment construction rate on the behaviour of GRWGC column-supported embankments is discussed in this section. The embankment construction rate was varied from 0.025 m/day to 0.2 m/day to replicate a complete range of construction sequences, from slow to fast, applicable in the field. According to Fig. 19 (a), (b) and (f), the construction rate does not have any significant effect on the SCR, AR and tension in the geogrid, which are the governing parameters of the load transfer mechanism of column-supported embankments. With increasing construction rate, maximum and differential settlements shown in Fig. 19 (c) and (d) decreased due to low effective stresses in the

foundation soil because the time was not sufficient to dissipate excess pore water pressures. In contrast to settlements, a slight increase in lateral displacement at the embankment toe was observed with the increasing embankment construction rate, as shown in Fig. 19 (e). The reduced resistance to lateral deformation at the toe is due to higher excess pore pressures in the soil at the end of construction, resulting from the increased construction rate of the embankment.

The long-term behaviour of SCR is marginally higher compared to short-term behaviour, as shown in Fig. 19(a). AR slightly decreased for the long-term case, indicating improved arching efficiency with consolidation, as depicted in Fig. 19(b). For the long-term case, settlements shown in Fig. 19(c) and (d) are higher than those for the short-term due to increased effective stresses with pore pressure dissipation. As a result, the tension in the geogrid has slightly increased, as illustrated in Fig. 19(f). The increased membrane action of the geogrid reduced lateral deformations at the embankment toe for the long-term case, as shown in Fig. 19 (e).

4.3.6 A simplified design guideline

The parametric study conducted in the previous section demonstrated the influence of five main design parameters: (i) column spacing, (ii) column diameter, (iii) tensile stiffness of the geogrid, (iv) embankment height and (v) embankment construction rate on six primary performance parameters: (i) SCR, (ii) AR, (iii) maximum total settlements, (iv) maximum differential settlements, (v) lateral displacement at the embankment toe and (vi) maximum tension of the geogrid in GRWGC column-supported embankments. It is important to summarise the outcomes of this study into a simplified design guideline that includes the influence of each design parameter on performance-evaluating parameters.

The ranking system introduced by Huang and Han (2010) provides a simplified guideline that quantifies the influence of each design parameter on the criteria used to evaluate the performance of GRWGC column-supported embankments. The Degree of Influence (DOI) factor was introduced in their study as the absolute difference between the maximum and minimum values of a parameter, expressed as a percentage of the average of the maximum and minimum values. Also, three influence levels were defined to categorise the degree of influence provided by the considered parameter: High (DOI > 60%), medium (30% < DOI < 60%) and low (DOI < 30%). In addition, a sign convention was introduced here to convey the type of impact enforced by the considered design parameter on the overall performance of the GRWGC column-supported embankments. Here, if the increasing design parameter positively impacts the performance of the GRWGC column-supported embankment, it is regarded as a positive (+) impact, and if it negatively impacts the performance of the GRWGC column-supported embankment, it is regarded as a negative (-) impact. Therefore, if the increasing design parameter increases the SCR, it is regarded as a positive (+) impact, and if it decreases the SCR, it is regarded as a negative (-) impact. Conversely, if the increasing design parameter decreases the AR, the maximum settlement, the maximum

differential settlement, lateral displacement at the embankment toe and the geogrid tension, it is regarded as a positive (+) impact, and if it increases them, it is considered a negative (-) impact.

Based on the parametric study, DOI factors, influence levels and impact types are summarised in Table 8 for both short-term and long-term behaviour, serving as a simplified design guideline. The tensile stiffness of the geogrid and the embankment construction rate have a relatively low impact on the embankment performance, as they are ranked as 'low' in most cases. The reason may be the higher embankment loads transferred to stiff GRWGC columns, compared to the soft clay. The column spacing, column diameter and embankment height strongly influence the performance of GRWGC column-supported embankments and can be considered as the most critical design parameters, concluding that the GRWGC columns predominantly govern the overall embankment behaviour.

Table 8: Summary of the results from the parametric study

	SCR		**AR**		**S_{max}**		**DS_{max}**		**L**		**T_{max}**	
	ST	**LT**	**ST**	**LT**	**ST**	**LT**	**ST**	**LT**	**ST**	**LT**	**ST**	**LT**
s	48 (M+)	54 (M+)	102 (H-)	92 (H-)	85 (H-)	95 (H-)	114 (H-)	125 (H-)	81 (H-)	84 (H-)	150 (H-)	153 (H-)
d_c	36 (M-)	45 (M-)	125 (H+)	123 (H+)	91 (H+)	102 (H+)	112 (H+)	123 (H+)	136 (H+)	131 (H+)	156 (H+)	157 (H+)
J	9 (L+)	12 (L+)	4 (L+)	4 (L+)	1 (L+)	1 (L+)	3 (L+)	2 (L+)	41 (M+)	49 (M+)	188 (H-)	187 (H-)
h_{emb}	38 (M+)	39 (M+)	32 (M-)	38 (M-)	124 (H-)	126 (H-)	125 (H-)	113 (H-)	148 (H-)	157 (H-)	153 (H-)	154 (H-)
CR	3 (L-)	5 (L-)	7 (L-)	7 (L-)	17 (L-)	1 (L-)	31 (M-)	1 (L-)	22 (L-)	17 (L-)	3 (L-)	0 (L-)

SCR- Stress concentration Ratio, AR- Arching ratio, S_{max}- Maximum settlement at the embankment base, DS_{max}-Maximum differential settlement at the embankment base, L- Lateral displacement of the embankment toe, T_{max}- Maximum tension of the geogrid, ST- Short-term, LT- Long-term, s- Column spacing, d_c- Column diameter, J- Tensile stiffness of the geogrid, h_{emb}- Height of the embankment, CR- Construction rate of the embankment

5. Conclusion

The research presented in this paper focused on three main objectives regarding the application of geopolymer-bound recycled waste glass aggregate composite (GRWGC) columns as embankment support: (i) Developing a constitutive model for the GRWGC material, (ii) Comparison of the performance of stone and GRWGC column-improved ground and (iii) Parametric study on GRWGC column-supported embankments to develop a simplified design guideline.

The strain-softening behaviour observed during triaxial tests of the GRWGC was incorporated into ABAQUS/Standard finite element software as an extension to the Mohr-Coulomb constitutive model using the user-defined field subroutine (USDFLD). The numerically simulated results of two-dimensional axisymmetric consolidated drained triaxial tests, using the proposed constitutive model, exhibited a good agreement with the stress-strain behaviour of the GRWGC, confirming the capability of the proposed model in simulating the GRWGC material behaviour.

A well-documented stone column-improved case study from Itaguaí District, Rio de Janeiro, Brazil, was selected to validate the numerical model and to compare the performance of stone and GRWGC column-improved ground. The measured settlement, lateral deformation and excess porewater pressure data were used for the model validation and showed excellent agreement with the field data. When using GRWGC columns to evaluate the performance against stone columns, due to the high stiffness of the GRWGC columns, the analysis could not be completed due to punching shear failure at the column toes positioned in clay. Therefore, the performance evaluation with stone columns was conducted by extending all columns by 2.95 m and positioning them in the sand layer located immediately after the clay layer. The simulations were conducted using 1 m diameter stone columns and GRWGC columns with diameters 1 m, 0.5 m and 0.25 m. Results show significant reductions in both settlements and lateral deformations for ground improved with all three diameters of GRWGC columns. A 78.1% settlement reduction and an 80.1% lateral deformation reduction were observed in the ground improved with 0.25 m diameter GRWGC columns in comparison to those of 1 m diameter stone columns. These results confirm that with increasing column diameter, the performance of the GRWGC column-improved ground shows significant improvements. Therefore, it can be concluded that GRWGC columns perform significantly better than unbound stone columns due to the high stiffness and improved properties achieved by binding glass aggregates with the geopolymer-based binder.

A parametric study was performed for GRWGC column-supported embankments investigating the impact of five design parameters: (i) column spacing, (ii) column diameter, (iii) tensile stiffness of the geogrid, (iv) embankment height, and (v) embankment construction rate on six performance evaluating parameters: (i) stress concentration ratio (SCR), (ii) arching ratio (AR), (iii) maximum settlement, (iv) maximum differential settlement, (v) lateral displacement at the embankment toe and (vi) maximum tension of the geogrid. The impacts of variations in these design parameters on the evaluation parameters were numerically represented using a degree of influence (DOI) factor. The influence of each design parameter was categorised into high, medium and low based on the calculated DOI for the evaluating parameter. Also, the type of impact on the embankment performance was indicated using a sign convention, denoting positive and negative impacts. The results from the simulations were comprehensively summarised with the DOI factor, influence category, and sign convention for both short-term and long-term behaviour, providing a simplified design guideline for

GRWGC column-supported embankments. This summary underscores the significant influence of column spacing, column diameter and embankment height on the overall performance of the GRWGC column-supported embankments.

6. References

Almeida, M., Lima, B., Riccio, M., Jud, H., and Roza, F. (2014). "Stone columns field test: monitoring data and numerical analyses." *Geotechnical Engineering Journal of the SEAGS & AGSSEA*, 45(1), 103-112.

Almeida, M. S. S., Hosseinpour, I., and Lima, B. (2019). "Field studies of stone columns and geosynthetic-encased columns." *From Research to Applied Geotechnics*, IOS Press, 166-180.

Ambily, A. P., and Gandhi, S. R. (2007). "Behavior of stone columns based on experimental and FEM analysis." *Journal of geotechnical and geoenvironmental engineering*, 133(4), 405-415.

Balaam, N. P., and Booker, J. R. (1981). "Analysis of rigid rafts supported by granular piles." *International journal for numerical and analytical methods in geomechanics*, 5(4), 379-403.

Black, J. A., Sivakumar, V., Madhav, M. R., and Hamill, G. A. (2007). "Reinforced stone columns in weak deposits: laboratory model study." *Journal of Geotechnical and Geoenvironmental Engineering*, 133(9), 1154-1161.

Borges, J. L., and Marques, D. O. (2011). "Geosynthetic-reinforced and jet grout column-supported embankments on soft soils: Numerical analysis and parametric study." *Computers and Geotechnics*, 38(7), 883-896.

Castro, J. (2017). "Modeling stone columns." *Materials*, 10(7), 782.

Castro, J., and Sagaseta, C. (2011). "Deformation and consolidation around encased stone columns." *Geotextiles and Geomembranes*, 29(3), 268-276.

Dheerendra Babu, M. R., Nayak, S., and Shivashankar, R. (2013). "A critical review of construction, analysis and behaviour of stone columns." *Geotechnical and Geological Engineering*, 31, 1-22.

Dutta, S., Padade, A. H., and Mandal, J. N. "Experimental study on natural bamboo geogrid encased stone column." *Proc., Proc., 5th Asian Regional Conf. on Geosynthetics, Geosynthetics Asia*, 417-426.

Foda, T., Hassan, H. M., Abdelkader, A., and el-Hassan, K. A. (2024). "Predictive modeling of sustainable recycled materials for stone column construction." *Innovative Infrastructure Solutions*, 9(11), 408.

Gharavi, H., Yazdani, E., Alidoust, P., Shariatmadari, N., Yazdani, F., and Niavol, K. P. (2023). "Utilization of shredded waste tire as a substitute for gravel in stone column groups." *KSCE Journal of Civil Engineering*, 27(1), 198-206.

Guo, R., and Li, G. (2008). "Elasto-plastic constitutive model for geotechnical materials with strain-softening behaviour." *Computers & geosciences*, 34(1), 14-23.

Han, J. (2015). *Principles and practice of ground improvement*, John Wiley & Sons.

Han, J., and Gabr, M. A. (2002). "Numerical analysis of geosynthetic-reinforced and pile-supported earth platforms over soft soil." *Journal of geotechnical and geoenvironmental engineering*, 128(1), 44-53.

Huang, J., and Han, J. (2010). "Two-dimensional parametric study of geosynthetic-reinforced column-supported embankments by coupled hydraulic and mechanical modeling." *Computers and Geotechnics*, 37(5), 638-648.

Hugher, J., and Withers, N. (1974). "Reinforcing of soft cohesive soils with stone columns." *Ground engineering*, 7(3), 42-49.

Kazmi, D., Serati, M., Williams, D. J., Olaya, S. Q., Qasim, S., Cheng, Y. P., Grizi, A., and Javadi, A. A. (2024). "Shear Strength and Consolidation Behaviour of Kaolin Clay Reinforced with a Granular Column Backfilled with Crushed Waste Glass." *Geotechnical and Geological Engineering*, 42(5), 3615-3632.

Liu, H., Kong, G., Chu, J., and Ding, X. (2015). "Grouted gravel column-supported highway embankment over soft clay: case study." *Canadian Geotechnical Journal*, 52(11), 1725-1733.

Malarvizhi, S. N. (2007). "Comparative study on the behavior of encased stone column and conventional stone column." *Soils and foundations*, 47(5), 873-885.

Mazumder, T., Rolaniya, A. K., and Ayothiraman, R. (2018). "Experimental study on behaviour of encased stone column with tyre chips as aggregates." *Geosynthetics International*, 25(3), 259-270.

Mitchell, J. K., and Huber, T. R. (1985). "Performance of a stone column foundation." *Journal of Geotechnical Engineering*, 111(2), 205-223.

Potts, D. M., Kovacevic, N., and Vaughan, P. R. (1997). "Delayed collapse of cut slopes in stiff clay." *Géotechnique*, 47(5), 953-982.

Prematilaka, K. K. W., and Liyanapathirana, D. S. (2026). "Geopolymer-Bound Recycled Waste Glass Aggregate Composite for Stone Columns: Geotechnical Properties and Durability." *Proceedings of the Institution of Civil Engineers - Ground Improvement, 1–13, https://doi.org/10.1680/jgrim.25.01011.*

Prematilaka, K. K. W., Liyanapathirana, D. S., and Leo, C. J. (2026). "A novel geopolymer-based composite material from recycled waste glass." *Journal of Materials in Civil Engineering*, ASCE, 38(3), 04025584:1-16, *https://doi.org/10.1061/JMCEE7.MTENG-20012*.

Prematilaka, K. K. W., Liyanapathirana, D. S., Leo, C. J., and Hu, P. (2024). "Application of recycled waste glass to replace traditional quarried aggregates: A comprehensive review." *Journal of Building Engineering*, 108846.

Shahverdi, M., and Haddad, A. (2020). "Use of recycled materials in floating stone columns." *Proceedings of the Institution of Civil Engineers-Construction Materials*, 173(2), 99-108.

Shariatmadari, N., Zeinali, S. M., Mirzaeifar, H., and Keramati, M. (2018). "Evaluating the effect of using shredded waste tire in the stone columns as an improvement technique." *Construction and Building Materials*, 176, 700-709.

Shen, P., Tang, H., Ning, Y., and Xia, D. (2019). "A damage mechanics based on the constitutive model for strain-softening rocks." *Engineering Fracture Mechanics*, 216, 106521.

Shivashankar, R., Dheerendra Babu, M. R., Nayak, S., and Manjunath, R. (2010). "Stone columns with vertical circumferential nails: laboratory model study." *Geotechnical and Geological Engineering*, 28, 695-706.

Tranter, R., Jefferson, I., and Ghataora, G. (2008). "The use of recycled aggregate in vibro-stone columns—a UK perspective." *GeoCongress 2008: Characterization, Monitoring, and Modeling of GeoSystems*, 630-637.

Troncone, A. (2005). "Numerical analysis of a landslide in soils with strain-softening behaviour." *Geotechnique*, 55(8), 585-596.

Wang, S., Yin, X., Tang, H., and Ge, X. (2010). "A new approach for analyzing circular tunnel in strain-softening rock masses." *International journal of rock mechanics and mining sciences*, 47(1), 170-178.

Wijerathna, M., and Liyanapathirana, D. S. (2021). "Numerical issues in modelling DCM column-supported embankments featuring post-yield strain-softening: 2D simplified vs 3D models." *International Journal of Geotechnical Engineering*, 15(7), 857-866.

Yapage, N. N. S., Liyanapathirana, D. S., Poulos, H. G., Kelly, R. B., and Leo, C. J. (2015). "Numerical modeling of geotextile-reinforced embankments over deep cement mixed columns incorporating strain-softening behavior of columns." *International Journal of Geomechanics*, 15(2), 04014047.